



ELSEVIER

Contents lists available at ScienceDirect

# Linear Algebra and its Applications

[www.elsevier.com/locate/laa](http://www.elsevier.com/locate/laa)



## Sampling method based projection approach for the reconstruction of 3D acoustically penetrable scatterers



Fermín S.V. Bazán<sup>a</sup>, Andreas Kleefeld<sup>b</sup>, Koung Hee Leem<sup>c</sup>,  
George Pelekanos<sup>c,\*</sup>

<sup>a</sup> Department of Mathematics, Federal University of Santa Catarina, Florianópolis SC, Santa Catarina, CEP 88040-900, Brazil

<sup>b</sup> Department I (Mathematics, Natural Sciences, Computer Science), Brandenburgische Technische Universität, 03013 Cottbus, Germany

<sup>c</sup> Department of Mathematics and Statistics, Southern Illinois University, Edwardsville, IL 62026, USA

### ARTICLE INFO

#### Article history:

Received 11 January 2015

Accepted 23 December 2015

Available online xxxx

Submitted by V. Mehrmann

#### MSC:

15A29

45B05

65J22

65F22

65M32

65R20

65R30

#### Keywords:

Linear sampling method

Factorization method

Acoustic scattering

### ABSTRACT

We present a projection based regularization parameter choice approach within the framework of the linear sampling method for the reconstruction of acoustically penetrable objects. Using the Golub–Kahan bidiagonalization algorithm and the Lanczos tridiagonalization process we form appropriate subspaces which generate a sequence of regularized solutions. As a result two new and efficient methods are developed and used for the solution of problems that involve large linear systems of equations. The effectiveness of our approach is illustrated with reconstructions of three dimensional objects.

© 2016 Elsevier Inc. All rights reserved.

\* Corresponding author.

E-mail addresses: [fermin@mtm.ufsc.br](mailto:fermin@mtm.ufsc.br) (F.S.V. Bazán), [kleefeld@tu-cottbus.de](mailto:kleefeld@tu-cottbus.de) (A. Kleefeld), [kleem@siue.edu](mailto:kleem@siue.edu) (K.H. Leem), [gpeleka@siue.edu](mailto:gpeleka@siue.edu) (G. Pelekanos).

## 1. Introduction

In this work, we will deal with reconstructions of acoustically penetrable objects from far-field measurements. This problem was originally investigated by Anagnostopoulos et al. [1] within the framework of the factorization method. Our goal will be to construct a robust and effective algorithm that will be able to handle acoustically penetrable objects that exhibit large linear systems of equations via the linear sampling method originally developed by Colton and Kirsch [11].

It is widely known that the linear sampling method does not require *a priori* information about either the boundary condition or the connectivity of the scatterer, however requires knowledge of the far-field pattern for all incident and observation directions. Hence, the cost of reconstructing three dimensional objects via the linear sampling method (LSM) could be prohibitively expensive if the discretization involves the construction of large systems of equations. In addition, due to the ill-posedness of the inverse problem, the linear sampling method yields an ill-conditioned system of linear equations whose solution requires a regularization method in order to handle correctly the presence of noise in the data. Moreover, the noise level in the data should be known *a priori*, something that in real life applications is not the case in general.

In our approach we will use an appropriate projection method that through the LSM will construct stable approximations to the far-field equation. Due to noise in the data however, it is necessary to combine our projection method with a regularization method like Tikhonov's regularization equipped with Morozov's generalized discrepancy principle as parameter choice rule which generally involves the computation of the zeros of the discrepancy function at each point of the grid. For large systems however, SVD-based methods, like the latter may be prohibitive due to the huge amount of data.

In the sequel, we will introduce two methods whose main idea will be to approximate the regularized solution by using a sequence of regularized solutions in appropriate Krylov subspaces of increasing dimension generated by projection methods such as Golub–Kahan bidiagonalization (GKB) [18, Section 8.6.2] and Lanczos tridiagonalization methods [18, Chapter 9]. Therefore, we will be taking advantage of the fact that the regularization parameter for the projected problem, which involves a small number of variables, can be determined efficiently and at low computational cost using a direct method such as the SVD of a small matrix. The first parameter estimation method will be called PGDP-FP (Projected Generalized Discrepancy Principle Fixed Point method) and will enable the widely used Morozov's discrepancy principle method to effectively provide regularization parameters, for problems that involve large linear systems of equations, as roots of a projected discrepancy function. Taking into account that GDP can fail when the noise level is not accurately estimated, we developed a second method that

does not rely on this estimate called PIMPC-FP (Projected Improved Maximum Product Criterion Fixed Point method). PIMPC-FP is an improved version of the IMPC (Improved Maximum Product Criterion) for large-scale problems, that has been developed by Bazán et al. [5] and has been proven to provide reliable reconstructions of medium size objects without *a priori* knowledge of the noise level.

We organize our paper as follows. In section 2, we formulate the direct and inverse scattering problems and introduce the far-field operator. Section 3 describes the main idea of the projection approach within the framework of the LSM, and the selection of the regularization parameter as a sequence of regularized solutions in appropriate Krylov subspaces is discussed in section 4. In sections 5 and 6 the authors apply the idea of projections on GDP and IMPC by generating appropriate subspaces via the Golub–Kahan bidiagonalization algorithm. As a result two new and efficient methods are generated for the reconstruction of acoustically penetrable objects that exhibit large scale far-field matrices, the PGDP-FP and the PIMPC-FC. Section 7 repeats the analysis presented in the previous two sections, but now focusing on a projection approach for Kirsch’s method based on the Krylov subspace generated by the Lanczos tridiagonalization method. Moreover, an extended discussion of the numerical implementation of our methods, along with various three dimensional reconstructions of objects will be included in section 8. Finally, conclusions will be presented in section 9 as well as possible future research.

## 2. Formulation of the direct and inverse scattering problem

In this section, we briefly formulate the direct and inverse acoustic scattering problem. We closely follow the description of [1] and refer the reader to [1] for more details.

First, we let  $D \subset \mathbb{R}^3$  be a bounded domain with sufficiently smooth boundary  $\partial D$ . We denote by  $\hat{\nu}$  the unit normal vector to the boundary  $\partial D$  which is assumed to be directed into the exterior of  $D$ . The exterior  $\mathbb{R}^3 \setminus \bar{D}$  of the scatterer is assumed to be connected. It is an infinite homogeneous isotropic non-absorbing acoustic medium characterized by mass density  $\rho_e$ , mean compressibility  $\kappa_e$ , and sound speed  $c_e = 1/\sqrt{\kappa_e \rho_e}$ . The medium occupying the interior of the scatterer  $D$  is characterized similarly by the parameters  $\rho_i$ ,  $\kappa_i$ , and  $c_i = 1/\sqrt{\kappa_i \rho_i}$ . The scatterer is excited by a time-harmonic acoustic plane wave

$$u^{\text{inc}}(\mathbf{x}; \hat{\mathbf{d}}) = e^{ik_e \mathbf{x} \cdot \hat{\mathbf{d}}}, \quad \mathbf{x} \in \mathbb{R}^3, \tag{1}$$

propagating in the direction  $\hat{\mathbf{d}} \in \mathbb{S}^2$  of unit length, where  $\mathbb{S}^2 := \{\mathbf{x} \in \mathbb{R}^3: |\mathbf{x}| = 1\}$  denotes the unit sphere, and where  $k_e = \omega/c_e$  is the wave number of the acoustic waves in the host medium.

The interference of the incident wave (1) with the penetrable scatterer leads to the creation of two secondary fields. The first is the scattered field  $u^{\text{sct}}(\mathbf{x})$ , which is defined in the exterior and it propagates outwards. The second is the transmitted field  $u^{\text{int}}(\mathbf{x})$ , which is defined in the interior of the scattering obstacle. The total acoustic field in the

exterior of the scatterer is given by the superposition of the scattered and the incident field.

Now, we briefly describe the *direct acoustic transmission scattering problem, transmission problem* (TP) for short. Find the two functions  $u^{\text{int}} \in C^2(D) \cap C^1(\bar{D})$  and  $u^{\text{sct}} \in C^2(\mathbb{R}^3 \setminus \bar{D}) \cap C^1(\mathbb{R}^3 \setminus D)$  satisfying the two Helmholtz equations

$$\Delta u^{\text{int}}(\mathbf{x}) + k_i^2 u^{\text{int}}(\mathbf{x}) = 0, \quad \mathbf{x} \in D, \tag{2}$$

$$\Delta u^{\text{sct}}(\mathbf{x}) + k_e^2 u^{\text{sct}}(\mathbf{x}) = 0, \quad \mathbf{x} \in \mathbb{R}^3 \setminus \bar{D}, \tag{3}$$

with the two transmission boundary conditions

$$u^{\text{int}}(\mathbf{x}) - u^{\text{sct}}(\mathbf{x}) = u^{\text{inc}}(\mathbf{x}), \quad \mathbf{x} \in \partial D, \tag{4}$$

$$\tau^{-1} \frac{\partial u^{\text{int}}}{\partial \hat{\nu}}(\mathbf{x}) - \frac{\partial u^{\text{sct}}}{\partial \hat{\nu}}(\mathbf{x}) = (\partial u^{\text{inc}} / \partial \hat{\nu})(\mathbf{x}), \quad \mathbf{x} \in \partial D, \tag{5}$$

and the Sommerfeld radiation condition

$$\lim_{r \rightarrow \infty} r \left( \frac{\partial u^{\text{sct}}(\mathbf{x})}{\partial r} - ik_e u^{\text{sct}}(\mathbf{x}) \right) = 0, \quad r = |\mathbf{x}|, \tag{6}$$

where  $k_i = \omega/c_i$  and  $k_e = \omega/c_e$  are the wave numbers of the acoustic medium filling the interior of  $D$  and of the host medium, respectively. Here,  $\tau := \rho_i/\rho_e \in \mathbb{R}^+$  is the mass density ratio of the two media. It is well known that problem (2)–(6) constitutes a well-posed BVP [13,15,26].

The problem at hand can be solved by using *Green’s representation formula*, since any radiating solution  $v \in C^2(\mathbb{R}^3 \setminus \bar{D}) \cap C^1(\mathbb{R}^3 \setminus D)$  to the Helmholtz equation can be represented by (see [14, Theorem 2.4])

$$v(\mathbf{x}) = \int_{\partial D} \left[ v(\mathbf{y}) \frac{\partial \Phi_a(\mathbf{x}, \mathbf{y})}{\partial \hat{\nu}(\mathbf{y})} - \frac{\partial v}{\partial \hat{\nu}}(\mathbf{y}) \Phi_a(\mathbf{x}, \mathbf{y}) \right] ds(\mathbf{y}), \quad \mathbf{x} \in \mathbb{R}^3 \setminus \bar{D}, \tag{7}$$

where  $\Phi_a(\mathbf{x}, \mathbf{y})$ ,  $a = \{e, i\}$  denotes the fundamental solution of the Helmholtz equation with wavenumber  $k_a$ . It is given by

$$\Phi_a(\mathbf{x}, \mathbf{y}) = \frac{e^{ik_a |\mathbf{x} - \mathbf{y}|}}{4\pi |\mathbf{x} - \mathbf{y}|}, \quad \mathbf{x}, \mathbf{y} \in \mathbb{R}^3, \quad \mathbf{x} \neq \mathbf{y}. \tag{8}$$

The far-field pattern of  $\Phi_e(\mathbf{x}, \mathbf{y})$  is given by (see [14, Theorem 2.5])

$$\Phi_e^\infty(\hat{\mathbf{x}}, \mathbf{y}) := \frac{1}{4\pi} \exp\{-ik_e \hat{\mathbf{x}} \cdot \mathbf{y}\}. \tag{9}$$

Hence, the far-field pattern  $u^\infty: \mathbb{S}^2 \times \mathbb{S}^2 \rightarrow \mathbb{C}$  is calculated by (see [14, Theorem 2.5])

$$u^\infty(\hat{\mathbf{x}}; \hat{\mathbf{d}}) = \frac{1}{4\pi} \int_{\partial D} \left[ u^{\text{sct}}(\mathbf{y}; \hat{\mathbf{d}}) \frac{\partial e^{-ik_e \hat{\mathbf{x}} \cdot \mathbf{y}}}{\partial \hat{\nu}(\mathbf{y})} - \frac{\partial u^{\text{sct}}(\mathbf{y}; \hat{\mathbf{d}})}{\partial \hat{\nu}(\mathbf{y})} e^{-ik_e \hat{\mathbf{x}} \cdot \mathbf{y}} \right] ds(\mathbf{y}), \quad \hat{\mathbf{x}} \in \mathbb{S}^2. \tag{10}$$

Next, we briefly describe the *inverse acoustic transmission scattering problem* as follows. Given the far-field patterns  $u^\infty(\hat{\mathbf{x}}; \hat{\mathbf{d}})$  for scattering from an isotropic and homogeneous penetrable scatterer for all directions of observation  $\hat{\mathbf{x}} \in \mathbb{S}^2$  and all directions of incidence  $\hat{\mathbf{d}} \in \mathbb{S}^2$ , the purpose is to reconstruct the shape of the unknown scatterer  $D$ . Note that from the theoretical point of view this inverse problem is uniquely solvable (see [25]).

A key ingredient for the solution of this inverse problem is the linear integral operator

$$(\mathcal{F}g)(\hat{\mathbf{x}}) := \int_{\mathbb{S}^2} u^\infty(\hat{\mathbf{x}}; \hat{\mathbf{d}})g(\hat{\mathbf{d}}) \, ds(\hat{\mathbf{d}}), \quad \hat{\mathbf{x}} \in \mathbb{S}^2, \tag{11}$$

henceforth called the far-field operator, where the kernel is formed by the far-field patterns. Note that this operator is compact, since the far-field pattern is an analytic function in both of its variables. The Linear Sampling method (LSM) looks for a function  $g \in L^2(\mathbb{S}^2)$  such that

$$(\mathcal{F}g)(\hat{\mathbf{x}}) = \Phi_e^\infty(\hat{\mathbf{x}}, \mathbf{z}), \quad \hat{\mathbf{x}} \in \mathbb{S}^2 \tag{12}$$

has a solution, where  $\mathbf{z}$  is an arbitrarily chosen sampling point. Roughly, for a set of sampling points  $\mathbf{z} \in \mathbb{R}^3$ , the Linear Sampling method looks for the solution of the far-field equation (12), exploiting the fact that the norm of approximate solutions of the far-field equation becomes large when  $\mathbf{z} \rightarrow \partial D$  and can therefore be used as an indicator of the shape of  $D$ . However, we notice that, due to the compactness of the far-field operator, the problem of solving the far-field equation is ill-posed. Thus, in general this equation does not necessarily have any solution [12]. Even so it can be proved the existence of nearby solutions  $g_\epsilon(\cdot, \mathbf{z}) \in L^2(\Omega)$  in the sense that

$$\|\mathcal{F}g_\epsilon(\cdot, \mathbf{z}) - \Phi_e^\infty(\cdot, \mathbf{z})\| \leq \epsilon, \tag{13}$$

where  $\epsilon$  is a small parameter independent of  $\mathbf{z}$ , such that

$$\lim_{\substack{\mathbf{z} \rightarrow \partial D \\ \mathbf{z} \in D}} \|g_\epsilon\|_{L^2(\Omega)} = \infty. \tag{14}$$

Based on these results, the linear sampling method looks for stable solutions of the far-field equation obtained through some regularization method, looking for those solutions that blow up as  $\mathbf{z}$  approaches  $\partial D$ .

Another way to characterize the scatterer  $D$  is in terms of a range test due to Kirsch [24] involving an appropriate factorization of the far-field operator. In particular, the following linear operator equation is used in place of (12)

$$[(\mathcal{F}^* \mathcal{F})^{1/4}g](\hat{\mathbf{x}}) = \Phi_e^\infty(\hat{\mathbf{x}}, \mathbf{z}), \quad \hat{\mathbf{x}} \in \mathbb{S}^2, \tag{15}$$

and the range test reads “a grid point  $\mathbf{z} \in D$  if, and only if,  $\Phi_e^\infty(\hat{\mathbf{x}}, \mathbf{z}) \in \mathcal{R}((\mathcal{F}^* \mathcal{F})^{1/4})$ ”. In terms of a singular system of the far-field operator,  $\{\sigma_j^c, u_j^c, v_j^c\}$ ,  $j \in \mathbb{N}$ , a grid point  $\mathbf{z}$  satisfies the range test if, and only if, the series  $\sum_{j=1}^\infty |\beta_j^{(\mathbf{z})}|^2 / \sigma_j^c$  is convergent, where  $\beta_j^{(\mathbf{z})}$  stands for the Fourier coefficient of  $\Phi_e^\infty(\hat{\mathbf{x}}, \mathbf{z})$  with respect to  $v_j^c$ , in which case the solution of (15) is  $g_{\mathbf{z}} = \sum_{j=1}^\infty (\beta_j^{(\mathbf{z})} / \sqrt{\sigma_j^c}) u_j^c$ . Equivalently,  $\mathbf{z} \in D$  if, and only if,  $\|g_{\mathbf{z}}\|^2 = \sum_{j=1}^\infty |\beta_j^{(\mathbf{z})}|^2 / \sigma_j^c < \infty$ . Thus, the characterization of the object can be done by inspecting gridpoints  $\mathbf{z}$  for which the norm  $\|g_{\mathbf{z}}\|^2$  becomes arbitrarily large. However, due to the compactness of the far-field operator, the problem of solving (15) is also ill-posed and some regularization is needed in order to compute stable solutions. The same idea is followed when Kirsch’s method is implemented in a finite dimensional framework.

### 3. Projection approach for the linear sampling method

The purpose of this section is to outline a projection approach for approximately solving the far-field equation through Tikhonov regularization, which will be the basis for our linear sampling method based projection approach for 3D object reconstruction. We start by considering the linear equation

$$\mathcal{A}g = h, \tag{16}$$

where  $\mathcal{A}$  is a linear and bounded operator with non-closed range from a Hilbert space  $X$  into a Hilbert space  $Y$  and  $g$  is assumed to belong to the range space of  $\mathcal{A}$ . As this equation is ill-posed, regularization methods are required for its numerical treatment. Perhaps the most immediate way to generate stable approximations to  $g^\dagger = \mathcal{A}^\dagger h$ , is by a projection method where we approximate the space  $X$  by a finite-dimensional subspace  $X_k$  under the assumption that

$$X_1 \subset X_2 \subset \dots, \quad \text{with} \quad \overline{\bigcup_{k=1}^\infty X_k} = X, \tag{17}$$

and generate approximations to  $g^\dagger$  by determining the minimal norm solution to

$$\mathcal{A}_k g = h, \tag{18}$$

which we denote by  $g^{(k)}$ , where  $\mathcal{A}_k = \mathcal{A} \mathcal{P}_k$  and  $\mathcal{P}_k$  is the orthogonal projector of  $X$  onto  $X_k$ . Even if  $f^{(k)}$  does not converge to  $f^\dagger$  as  $k \rightarrow \infty$  in general, it turns out that when convergence holds and the subspace  $X_k$  is properly chosen, the most important features of  $f^\dagger$  are quickly captured for small  $k$  in  $g^{(k)}$ . For conditions that guarantee convergence of  $g^{(k)}$  to  $g^\dagger$  as  $k \rightarrow \infty$ , the reader is referred to Groetsch [19] and Engl et al. [16].

We emphasize that regularization is necessary when solving the far-field equation as in practice the integral operator is affected by measurement noise. Hence a projection approach as described before could be used in order to construct stable approximations to the solution of the far-field equation. However, it is well known that for noisy data, better results are obtained by combining the projection method with an additional regularization method such as Tikhonov regularization. The Tikhonov regularized solution to the ill-posed problem (16) is defined by

$$g_\lambda = \operatorname{argmin}_{g \in X} \{ \| \mathcal{A}g - h \|^2 + \lambda^2 \| g \|^2 \}, \tag{19}$$

where  $\lambda > 0$  is the regularization parameter. The regularization parameter determines how close  $g_\lambda$  is to the noise free solution of (16), and should therefore be carefully chosen. Postponing the choice of the regularization parameter to later on, for our projection approach we assume again that  $X_k$  is an expanding sequence of finite-dimensional subspaces of  $X$  whose union is dense in  $X$ . We can then generate finite-dimensional approximations  $g_\lambda^{(k)}$  to  $g^\dagger$  by minimizing the Tikhonov functional  $g \mapsto \| \mathcal{A}g - h \|^2 + \lambda^2 \| g \|^2$  over  $X_k$ . This problem is equivalent to solving the “projected problem”

$$g_\lambda^{(k)} = \operatorname{argmin}_{g \in X_k} \{ \| \mathcal{A}_k g - h \|^2 + \lambda^2 \| g \|^2 \}, \tag{20}$$

with  $\mathcal{A}_k$  and  $\mathcal{P}_k$  as before. For the case when the operator is free of noise it can be proved that  $g_\lambda^{(k)} \rightarrow \mathcal{A}^\dagger h$  as  $\lambda \rightarrow 0$  and  $k \rightarrow \infty$  simultaneously only if  $\lambda$  and  $k$  are related in a proper way, the success of this depending on how well  $\mathcal{A}_k$  approximates  $\mathcal{A}$ , or equivalently how quickly the number

$$\gamma_k = \| \mathcal{A}(I - \mathcal{P}_k) \| \tag{21}$$

becomes small. Obviously convergence is not an issue when we are dealing with discrete counterparts of the ill-posed problem (16) since in this case the linear operator has finite rank. However, for large-scale problems, the condition  $\gamma_k \approx 0$  will become crucial for the projection approach to be successful: the smaller the dimension of  $X_k$  for which  $\gamma_k \approx 0$ , the better the results of the projection approach. This is the central observation on which the projection approach is based.

We end the section with a very simple description of the linear sampling method based projection approach we have in mind. Basically, it comprises the following steps:

- (i) Choose a subspace  $X_k$ .
- (ii) For each grid point  $\mathbf{z}$  solve the projected problem (20) associated to either the far-field equation (12) or (15) in conjunction with an appropriate Tikhonov parameter choice rule.
- (iii) Determine the scatterer  $D$  by inspecting for which gridpoints  $\mathbf{z}$  the norm  $\| g_{\lambda, \mathbf{z}} \|$  becomes large.

The effectiveness of the projected approach will be demonstrated by numerical examples later.

**4. On the selection of the Tikhonov regularization parameter**

For the numerical realization of the linear sampling method the far-field equation has to be discretized. The main difficulty here is that, since the original problem is ill-posed, the linear system representing the discrete counterpart of (12) is ill-conditioned and characterized by numerical instability. Thus to obtain stable approximate solutions of the continuous problem, an appropriate regularization method should be used. Henceforth, we shall assume that the unit sphere is discretized using a triangular mesh containing  $N$  vertices (which are also used as directions for the plane incident waves) and that the far-field equation is discretized by following the scheme described in [10], giving rise to a system of  $N \times N$  linear equations

$$Fg_z = r_z, \quad F \in \mathbb{C}^{N \times N}, \tag{22}$$

where  $r_z \in \mathbb{C}^N$  is a discrete version of  $\Phi_e^\infty(\hat{x}, z)$  and  $F$  denotes the far-field matrix. Thus, for the implementation of the linear sampling method, the Tikhonov regularized solution is

$$g_{\lambda,z} = \underset{g \in \mathbb{C}^N}{\operatorname{argmin}} \{ \|\tilde{F}g - r_z\|_2^2 + \lambda^2 \|g\|_2^2 \} \tag{23}$$

where  $\lambda$  is the regularization parameter and  $\tilde{F}$  is a perturbed far-field matrix:  $\tilde{F} = F + E$ . The choice of  $\lambda$  has been made via Morozov’s generalized discrepancy principle (GDP) [9, 10,20]. GDP chooses as regularization parameter the only root of the nonlinear equation

$$G(\lambda) = \|\tilde{F}g_{\lambda,z} - r_z\|_2^2 - \delta_F^2 \|g_{\lambda,z}\|_2^2 = 0 \tag{24}$$

where  $\delta_F$  is an estimate for  $\|E\|$  such that  $\|E\| \leq \delta_F$ . The function  $G$  is increasing and has a unique root under mild conditions [28]. Additionally,  $G$  is convex for small  $\lambda$  and concave for large  $\lambda$ . As a result global and monotone convergence of Newton’s method cannot be guaranteed [32]. To overcome this difficulty, Lu et al. [28] transformed equation (24) into one that depends on two free parameters  $(\eta, \nu)$  and perform an analysis to determine the set of parameters that ensure global convergence of Newton’s method. Numerical examples reported in [28] suggest that among the pairs  $(\eta, \nu)$  that guarantee convergence, there must be a pair for which the iteration converges faster, but the determination of such a pair is still lacking.

GDP works well when  $\|E\|$  is accurately estimated but this may not be the case in real life applications. There exist some alternative parameter selection criteria that avoid knowledge of the noise level, referred to as heuristic rules, which have also been used in inverse scattering; these include the L-curve method [22,31] and a Fixed-point method

[2,27]. Recently, Fares et al. [17] developed a new heuristic algorithm, the SVD-tail, based on the combined presence of error in the operator and eigenvalue clusters corresponding to a singular subspace associated with a few small singular values. SVD-tail is proven efficient since the point-wise solution of the far-field equation is never explicitly constructed; one of its disadvantages though is that the quality of the reconstruction depends on the chosen dimension of the singular subspace.

More recently, Bazán et al. [7] introduced the so-called maximum product criterion (MPC) which defines as regularization parameter a solution to the problem

$$\bar{\lambda} = \operatorname{argmax}_{\lambda > 0} \{ \Psi(\lambda) \}, \quad \Psi(\lambda) = \mathbf{x}(\lambda) \mathbf{y}(\lambda), \tag{25}$$

where

$$\mathbf{y}(\lambda) = \|g_{\lambda, \mathbf{z}}\|^2, \quad \mathbf{x}(\lambda) = \|r_{\mathbf{z}} - \tilde{F}g_{\lambda, \mathbf{z}}\|_2^2. \tag{26}$$

Existence of a maximum is always guaranteed when the far-field matrix is nonsingular as in such a case  $\Psi(\lambda) \geq 0$  and  $\Psi(0) = 0 = \lim_{\lambda \rightarrow \infty} \Psi(\lambda)$ . The main virtue of MPC (illustrated on 2D reconstruction problems in [7]) is to deliver regularized solutions of large norm for  $\mathbf{z}$  outside  $D$  and regularized solutions of small norm for  $\mathbf{z}$  inside, a necessary condition for LSM to produce good reconstructions. From the practical point of view, under the assumption that  $\Psi$  has a unique maximizer, the authors in [7] show that such a maximizer can be determined by applying some root finder to the nonlinear equation

$$\varphi(\lambda) = \mathbf{x}(\lambda) - \lambda^2 \mathbf{y}(\lambda) = 0. \tag{27}$$

However, MPC can fail when the function  $\Psi$  has several local maxima. Difficulties arise since, depending on factors such as the chosen root finder, the chosen initial guess, etc., the regularization parameter determined in this way may not guarantee the success of LSM. To overcome these difficulties, Bazán et al. [3] introduced an improved version of MPC (IMPC) based on a fast fixed-point algorithm. For medium size problems, all the above selection criteria can be readily implemented using the singular value decomposition (SVD) of  $\tilde{F}$ .

Having reviewed current selection criteria for the Tikhonov regularization parameter in connection with inverse scattering, we will now concentrate on new algorithms for determining this parameter for the case when the far-field matrix is such that the use of SVD-based approaches is prohibitive, while the projection approach is well suited. As indicated in the Introduction, the main idea of our methods is to approximate the regularized solution  $g_{\lambda}$  by using a sequence of regularized solutions  $g_{\lambda}^{(k)}$  in appropriate Krylov subspaces of increasing dimension. By doing so, the regularization parameter for the projected problem will now involve only  $k$  variables, and can be determined efficiently at low computational cost using a direct method such as the SVD of a small matrix.

### 5. Linear sampling method based projection approach equipped with GDP

As already commented, when using GDP errors  $\delta_F$  are taken into account and the regularization parameter is chosen as the unique root of the equation  $G(\lambda) = 0$ . Existence and uniqueness of such solution follows as  $G$  is a monotonically increasing continuous function of  $\lambda$  since  $\mathbf{x}(\lambda)$  and  $\mathbf{y}(\lambda)$  are monotonic [7,3]. Thus,  $G$  will have a unique root as long as

$$\lim_{\lambda \rightarrow 0^+} G(\lambda) = \delta_0^2 - \delta_F^2 \|g_{LS}\|_2^2 < 0, \tag{28}$$

where  $g_{LS}$  denotes the unregularized solution of (22) and  $\delta_0$  denotes the norm of the incompatible component of  $r_z$  that lies outside the range subspace of  $\tilde{F}$ . Consequently, imposing the reasonable condition that  $\delta_F \ll \sigma_1(F)$ , the discrepancy equation  $G(\lambda) = 0$  will have a unique solution as long as the noise  $\delta_F$  satisfies

$$\frac{\delta_0}{\|g_{LS}\|_2} < \delta_F \ll \sigma_1(F). \tag{29}$$

If the far-field matrix  $\tilde{F}$  is nonsingular, as seen frequently when the noise is random, then  $\delta_0 = 0$  and the left inequality is satisfied automatically. The right inequality holds true when the amount of noise  $\delta_F$  is small. From here on we will assume that  $\tilde{F}$  is always nonsingular and concentrate on a method for solving the discrepancy equation. Let the singular value decomposition (SVD) of  $\tilde{F}$  be

$$\tilde{F} = U \Sigma V^H \tag{30}$$

where  $^H$  denotes conjugate transpose,  $U = [u_1, \dots, u_N]$ ,  $V = [v_1, \dots, v_N]$  are orthonormal matrices, and  $\Sigma = \text{diag}(\sigma_1, \dots, \sigma_N)$ , with  $\sigma_1 \geq \sigma_2 \geq \dots \geq \sigma_N$ . Based on the SVD of  $\tilde{F}$  and (26), the discrepancy equation is shown to be

$$G(\lambda) = \sum_{i=1}^N \frac{(\lambda^4 - \delta_F^2 \sigma_i^2) \alpha_i}{(\sigma_i^2 + \lambda^2)^2}, \tag{31}$$

where  $\alpha_i = |u_i^H r_z|^2$ . As already commented, this function is convex for small  $\lambda$  and concave for large  $\lambda$  and thus global convergence of Newton’s method cannot be guaranteed [32]. The following result shows that the unique root of the discrepancy equation can be computed through a fixed-point algorithm.

**Theorem 5.1.** For  $\lambda > 0$  let  $\vartheta(\lambda) = \frac{\|\tilde{F}g_\lambda - \tilde{r}_z\|_2}{\delta_F \|g_\lambda\|_2}$  and  $\zeta(\lambda) = \frac{\lambda}{\sqrt{\vartheta(\lambda)}}$ . Assume that (29) holds true. Then the following properties hold:

- a) The parameter chosen by GDP,  $\lambda_{GDP}$ , is the unique root of the nonlinear equation  $\vartheta(\lambda) = 1$ .

- b)  $\zeta$  is a monotonically increasing function having a unique nonzero fixed-point at  $\lambda = \lambda_{\text{GDP}}$  such that  $\zeta(\lambda) \geq \lambda$  if  $0 < \lambda \leq \lambda_{\text{GDP}}$ , and  $\zeta(\lambda) \leq \lambda$  if  $\lambda \geq \lambda_{\text{GDP}}$ .
- c) For given  $\lambda_0 > 0$  consider the sequence  $\{\lambda_j\}$  defined by

$$\lambda_{j+1} = \zeta(\lambda_j), \quad j \geq 0. \tag{32}$$

Then  $\lim_{j \rightarrow \infty} \lambda_j = \lambda_{\text{GDP}}$  irrespective of the initial guess chosen.

**Proof.** Recall from [3, Lemma 3.1] that both  $\vartheta(\lambda)$  and  $\zeta(\lambda)$  are increasing functions. Using this result together with the observation that  $\vartheta(\lambda) = 1$  is another way of writing (24) item a) follows.

For the proof of item b) we first notice that since  $\lambda_{\text{GDP}}$  is a solution of  $\vartheta(\lambda) = 1$ , then

$$\zeta(\lambda_{\text{GDP}}) = \frac{\lambda_{\text{GDP}}}{\sqrt{\vartheta(\lambda_{\text{GDP}})}} = \lambda_{\text{GDP}}.$$

This shows that  $\lambda_{\text{GDP}}$  is a fixed-point of  $\zeta$ . Conversely, if  $\lambda^*$  is a fixed-point of  $\zeta$ , which means  $\zeta(\lambda^*) = \lambda^*$ , then it follows that  $\vartheta(\lambda^*) = 1$  and, due to item a), we obtain  $\lambda^* = \lambda_{\text{GDP}}$ . This implies that  $\zeta$  has a unique nonzero fixed-point at  $\lambda = \lambda_{\text{GDP}}$ .

We now proceed with the observation that  $\zeta'(\lambda_{\text{GDP}}) < 1$ , which we prove by contradiction. In fact, assume  $\zeta'(\lambda_{\text{GDP}}) \geq 1$ . Then since  $\vartheta(\lambda_{\text{GDP}}) = 1$  by item a) and since

$$\zeta'(\lambda) = (\vartheta(\lambda))^{-1/2} - \frac{\lambda}{2} \vartheta'(\lambda) (\vartheta(\lambda))^{-3/2},$$

taking  $\lambda = \lambda_{\text{GDP}}$  we obtain

$$1 \leq \zeta'(\lambda_{\text{GDP}}) = 1 - \frac{\lambda_{\text{GDP}}}{2} \vartheta'(\lambda_{\text{GDP}}),$$

or equivalently  $\vartheta'(\lambda_{\text{GDP}}) \leq 0$ , which is a contradiction as  $\vartheta$  is increasing. Therefore we must have  $\zeta'(\lambda_{\text{GDP}}) < 1$ . Using this property, the monotonicity of  $\zeta$  and the fact  $\zeta$  has a unique nonzero fixed-point, we conclude that  $\zeta(\lambda) \geq \lambda$  if  $0 < \lambda \leq \lambda_{\text{GDP}}$  and  $\zeta(\lambda) \leq \lambda$  if  $\lambda \geq \lambda_{\text{GDP}}$ . This ends the proof of item b).

Finally, since  $\zeta$  is also an increasing function it follows that  $\{\lambda_k\}$  will be either an increasing sequence if  $\lambda_0 < \lambda_{\text{GDP}}$  or a decreasing sequence if  $\lambda_0 > \lambda_{\text{GDP}}$ . This concludes the proof.  $\square$

Our fixed-point algorithm for determining the regularization parameter  $\lambda_{\text{GDP}}$  can be outlined as follows.

**GDP-FP algorithm:**

**Input data:**  $\tilde{F}$ ,  $r_z$ ,  $\epsilon$ , and  $\delta_A$ .

1. Compute the SVD of  $\tilde{F}$ .
2. Set  $j = 0$  and take, e.g.,  $\lambda_0 = \sigma_1$ .
3. Compute  $\lambda_{j+1} = \zeta(\lambda_j)$  with  $\zeta$  being defined in [Theorem 5.1](#).
4. **If**  $|\lambda_{j+1} - \lambda_j| \geq \epsilon|\lambda_j|$   
**do**  $j \leftarrow j + 1$  and **go to** 3.  
**else** stop.
5. Compute  $g_{\lambda,z}$ .

Full computation of the SVD of  $\tilde{F}$  is quite expensive and thus unreliable for large-scale problems. For large-scale problems, we will see that projection methods are reliable options.

*5.1. General projection approach for computing regularization parameter chosen by GDP*

We shall now construct approximations to the regularized solutions  $g_{\lambda_{\text{GDP}},z}$  for the case where the dimension of the far-field matrix  $\tilde{F}$  is such that the computation of its SVD is infeasible or unattractive. As in Hilbert space settings, we consider an increasing sequence of  $k$ -dimensional subspaces  $X_k$  of  $\mathbb{C}^N$  and generate a sequence of approximations  $\tilde{\lambda}^{(k)}$  to  $\lambda_{\text{GDP}}$  by solving “the projected discrepancy equation”

$$G^{(k)}(\lambda) = \|\tilde{F}g_{\lambda,z}^{(k)} - r_z\|_2^2 - (\delta_F \|g_{\lambda,z}^{(k)}\|_2)^2 = 0, \tag{33}$$

where for  $\lambda > 0$  and  $k \geq 1$ ,  $g_{\lambda,z}^{(k)}$  solves the regularized projected problem

$$g_{\lambda,z}^{(k)} = \operatorname{argmin}_{g \in X_k} \left\{ \|\tilde{F}_k g - r_z\|^2 + \lambda^2 \|g\|^2 \right\} \tag{34}$$

in which  $\tilde{F}_k = \tilde{F}P_k$ , with  $P_k$  being the orthogonal projector onto the subspace  $X_k$ . Let  $\{u_j^{(k)}, \sigma_j^{(k)}, v_j^{(k)}\}$ ,  $j = 1, \dots, k$ , be a singular system for  $\tilde{F}_k$ . Then the projected discrepancy equation reads

$$G^{(k)}(\lambda) = \sum_{i=1}^k \frac{(\lambda^4 - \delta_F^2 [\sigma_i^{(k)}]^2) \alpha_i^{(k)}}{([\sigma_i^{(k)}]^2 + \lambda^2)^2} + [\delta_0^{(k)}]^2 = 0, \tag{35}$$

where  $\delta_0^{(k)}$  is defined in the same way as  $\delta_0$  is defined in (28) and  $\alpha_i^{(k)} = |u_j^{(k)H} r_z|^2$ . It is clear that for  $k \ll N$  evaluation of  $G^{(k)}(\lambda)$  will be significantly cheaper than evaluation of  $G(\lambda)$ . Thus, if  $G^{(k)}(\lambda)$  is close to  $G(\lambda)$  in some interval containing the root of  $G$  and  $k \ll N$ , good approximations to  $\lambda_{\text{GDP}}$  can be quickly obtained from (35). This justifies, to some extent, the use of the projection approach in solving large-scale problems. The

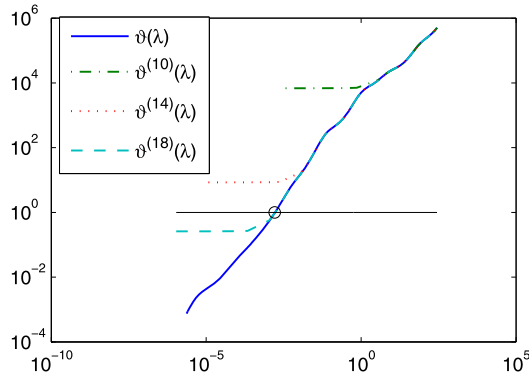


**Fig. 1.** Typical behavior of functions  $\vartheta(\lambda)$  and  $\vartheta^{(k)}(\lambda)$  for data from an inverse scattering problem with noisy far-field matrix of order  $512 \times 512$  such that  $\delta_F = \|\tilde{F} - F\|_2 = 2.5 \times 10^{-3}$ . The regularization parameter  $\lambda_{\text{GDP}}$  is marked with a small circle and obtained intersecting the curve  $z = \vartheta(\lambda)$  with the line  $z = 1$ .

success of this undertaking depends on a proper selection of the subspace  $X_k$  and on the simplicity as the projected problem is solved. As for the first requirement, a careful look at the functions  $G(\lambda)$  and  $G^{(k)}(\lambda)$  reveals that for these functions remain close to each other in a certain interval  $a \leq \lambda \leq \sigma_1$ , the singular  $\sigma_j$  contained in that interval must be approximated well by the singular values  $\sigma_j^k$ . In other words, what matters here is that the selection of the subspace  $X_k$  should be made so that the operator  $\tilde{F}_k$  can capture as many dominant singular values of  $\tilde{F}$  as possible.

To illustrate the potential of the projection approach in connection with GDP, for  $k \geq 1$  consider the sequence of functions  $\vartheta^{(k)} : \mathbb{R}^+ \rightarrow \mathbb{R}$ ,  $k = 1, \dots, N$ , defined by

$$\vartheta^{(k)}(\lambda) = \frac{\|r_z - \tilde{F}_k g_{\lambda,z}^{(k)}\|_2}{\delta_F \|g_{\lambda,z}^{(k)}\|_2} \equiv \frac{\rho^{(k)}(\lambda)}{\delta_F \eta^{(k)}(\lambda)}. \tag{36}$$

Notice that determining roots of the projected discrepancy equation is equivalent to determining roots of the nonlinear equation  $\vartheta^{(k)}(\lambda) = 1$  and that this equation may or may not have any root. However, we can deduce that a sufficient condition for the existence of roots of  $G^{(k)}(\lambda)$  is

$$\frac{\delta_0^{(k)}}{\|g_{\text{LS}}^{(k)}\|_2} < \delta_F \ll \sigma_1(F). \tag{37}$$

The promising potential of the projection approach is illustrated in Fig. 1 where for  $X_k$  we have selected the Krylov subspace  $\mathcal{K}_k(\tilde{F}^H \tilde{F}, \tilde{F}^H r_z)$  generated by the Golub–Kahan bidiagonalization (GKB) algorithm [8,18]. Notice that in a wide range of  $\lambda$  values which include the parameter  $\lambda_{\text{GDP}}$ , the functions  $\vartheta^{(k)}$  remain remarkably close to  $\vartheta$  even for small  $k$ . For this example, a subspace of dimension  $k = 18$  suffices to determine good approximation to the root of the original problem. A way to understand this success is by inspecting the closeness between the far-field matrix  $\tilde{F}$  and the projected one  $\tilde{F}_k = F P_k$

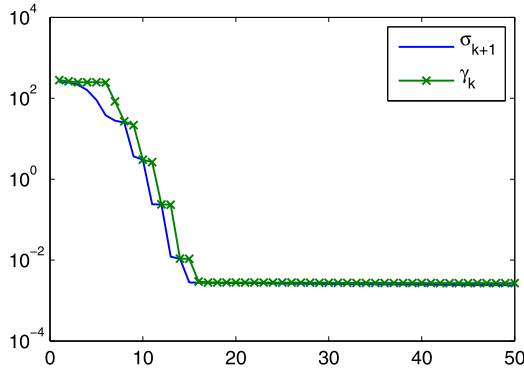


Fig. 2. Comparison of  $\sigma_{k+1}$  and  $\gamma_k$  for integer  $k$  ranging from 1 to 50.

as done by the number  $\gamma_k = \|\tilde{F} - \tilde{F}_k\|_2$ , see eq. (21). Number  $\gamma_k$  associated to the GKB algorithm has been investigated by Bazán et al. in [6]. The main conclusions of these authors is that  $\gamma_k$  decreases with  $k$ ,  $\gamma_k \geq \sigma_{k+1}$ , with the inequality becoming an equality when  $X_k$  is the dominant  $k$ -dimensional subspace generated by the first  $k$  right singular vectors of  $\tilde{F}$ . These properties are illustrated in Fig. 2. Notice that  $\gamma_k$  becomes small for moderate  $k$ ; this explains both the closeness between  $\vartheta^{(k)}$  and  $\vartheta$  for  $k = 18$  and for a range of  $\lambda$  values containing the regularization parameter  $\lambda_{GDP}$ , as seen in Fig. 1, and the success of the GKB algorithm when solving discrete ill-posed problems [4,22].

Besides the remarkable closeness between  $\tilde{F}_k$  and  $\tilde{F}$  for moderate  $k$ , perhaps the most important consequence of using the GKB algorithm in inverse scattering is that the information captured in the Krylov subspace can be used to implement the Linear Sampling method based on the computation of the roots of the projected discrepancy function, with the observation that the subspace needs to be calculated no more than once. Before we describe this implementation we will show how to efficiently solve the projected problem.

**Lemma 5.2.** *Let the columns of  $V_k$  form an orthonormal basis of the subspace  $X_k$ . Then the regularized solution  $g_{\lambda,z}^{(k)}$  and the corresponding residual  $r_{\lambda}^{(k)} = r_z - \tilde{F}y_{\lambda}^{(k)}$  satisfy*

$$g_{\lambda,z}^{(k)} = V_k y_{\lambda}^{(k)}, \quad y_{\lambda}^{(k)} = \left( V_k^H \tilde{F}^H \tilde{F} V_k + \lambda^2 I_k \right)^{-1} V_k^H \tilde{F}^H r_z, \tag{38}$$

$$r_{\lambda}^{(k)} = r_z - \tilde{F}_k g_{\lambda,z}^{(k)}. \tag{39}$$

Consequently,  $\|g_{\lambda,z}^{(k)}\|_2 = \|y_{\lambda}^{(k)}\|_2$ .

**Proof.** The regularized solution of the projected problem (34) reads

$$g_{\lambda,z}^{(k)} = \left[ (\tilde{F}P_k)^H (\tilde{F}P_k) + \lambda^2 I_N \right]^{-1} (\tilde{F}P_k)^H r_z. \tag{40}$$

Using the SVD it is straightforward to see that for each matrix  $A \in \mathbb{C}^{m \times n}$  it holds

$$(A^H A + \lambda I_n)^{-1} A^H = A^H (A A^H + \lambda I_m)^{-1}. \tag{41}$$

The assertion of the lemma in (38) follows by using the above property twice in (40). The assertion in (39) follows automatically.  $\square$

A brief description of LSM based on a general projected approach might go as follows.

---

**Linear Sampling Method based on GDP and a general projection approach (LSM-PGDP)**

---

1. Select a grid point  $z \in \mathbb{R}^3$ .
  2. Determine a subspace  $X_j$ ,  $j \geq 1$ , such that condition (37) is fulfilled and compute the root  $\lambda_{\text{GDP}}^{(j)}$  of  $G^{(j)}(\lambda)$ .
  3. Do  $j \leftarrow j + 1$ , repeat step 2 and stop when  $\lambda_{\text{GDP}}^{(j)}$  stagnates.
  4. After  $\lambda_{\text{GDP}}^{(j)}$  stagnates set  $k = j + p$ ,  $p \geq 0$ , and construct subspace  $X_k$ .
  5. Apply LSM to the regularized “projected problem” (34) with  $X_k$  as subspace.
- 

**Remark.** There are probably many ways to determine a subspace  $X_j$  required at step 2 of LSM-PGDP such that (37) is fulfilled. In our approach such a subspace is determined by solving a sequence of least squares problems  $g_{\text{LS}}^{(j)} = \operatorname{argmin}_{g \in X_j} \|\tilde{F}_k g - r_z\|^2$  through Krylov projection methods such as LSQR, MINRES, GMRES, etc. [29,18]. Interesting enough, these methods provide both the current approximate solution  $g_{\text{LS}}^{(j)}$  and the associated subspace  $X_j$ . Number  $p$  at step 4 is introduced to enhance the approximation properties of subspace  $X_k$  and can be chosen as  $p = 0$ . Enhancement is important since, as  $X_j$  is a Krylov subspace that depends on  $r_z$  for the chosen grid point  $z$ , the solution of the projected problem associated to other grid point may not be satisfactory if the dimension  $j$  is not increased in order to improve the information contained in the subspace. We will return to this point after our projection based approach for LSM is further discussed later on.

The main result of the section asserts that the regularization parameter  $\lambda_{\text{GDP}}$  can be approximated monotonically by a sequence of roots of  $\vartheta^{(k)}(\lambda)$  or equivalently by a sequence of fixed-points of a related function. This can be seen as follows. For fixed  $z$  let  $\zeta^{(k)} : \mathbb{R}^+ \rightarrow \mathbb{R}$ ,  $k = 1, \dots, N$ , be defined by

$$\zeta^{(k)}(\lambda) = \frac{\lambda}{\sqrt{\vartheta^{(k)}(\lambda)}}. \tag{42}$$

The following theorem describes how the sequence  $\zeta^{(k)}$  relates to the function  $\zeta$  of the original and large-scale problem and shows that  $\zeta^{(k)}$  always has a unique nonzero fixed-point that approximates  $\lambda_{\text{GDP}}$  from below.

**Theorem 5.3.** *Under the assumption that for  $\lambda > 0$*

$$\|g_\lambda^{(k+1)}\| \geq \|g_\lambda^{(k)}\|, \quad \|r_\lambda^{(k+1)}\| \leq \|r_\lambda^{(k)}\|, \quad k = 1, \dots, N - 1, \tag{43}$$

*we have that*

$$\vartheta^{(k+1)}(\lambda) \leq \vartheta^{(k)}(\lambda), \quad k = 1, \dots, N - 1, \tag{44}$$

$$\zeta^{(k+1)}(\lambda) \geq \zeta^{(k)}(\lambda), \quad k = 1, \dots, N - 1. \tag{45}$$

*Additionally, provided that condition (37) holds for some integer  $\widehat{k} \geq 1$ , for fixed  $\mathbf{z}$  and  $k \geq \widehat{k}$  we can generate a monotonic finite sequence of fixed points  $\{\bar{\lambda}^{(k)}\}$  of  $\zeta^{(k)}$  that converges to  $\lambda_{\text{GDP}}$  in at most  $N$  steps, where  $\bar{\lambda}^{(k)}$  is the unique solution of the nonlinear equation  $\vartheta^{(k)}(\lambda) = 1$ .*

**Proof.** Inequalities (44)–(45) are immediate consequences of (43). To prove the assertion concerning existence of fixed-point of  $\zeta^{(k)}$  we first notice that, since  $\rho^{(k)}$  and  $\eta^{(k)}$  are monotonic [2, Section 1], it follows that  $\vartheta^{(k)'}(\lambda) > 0$  and  $\zeta^{(k)'}(\lambda) > 0$ , see, e.g., [3, Lemma 3.1], and thus both  $\vartheta^{(k)}$  and  $\zeta^{(k)}$  are monotonically increasing functions. Next, since for  $k \geq \widehat{k}$  the nonlinear equation  $\vartheta^{(k)}(\lambda) = 1$  has a root by assumption, this root is unique due to  $\vartheta^{(k)}$  being increasing. But due to the definition of  $\zeta^{(k)}$  it follows that  $\bar{\lambda}^{(k)}$  is a fixed-point of  $\zeta^{(k)}$  if and only if  $\bar{\lambda}^{(k)}$  is the unique root of  $\vartheta^{(k)}(\lambda) = 1$ . This concludes the first part of the proof.

Now for given  $k \geq \widehat{k}$  and arbitrarily chosen initial guess  $\lambda_0^{(k)} > 0$ , consider the sequence  $\{\lambda_j^{(k)}\}$  defined by

$$\lambda_{j+1}^{(k)} = \zeta^{(k)}(\lambda_j^{(k)}), \quad j \geq 0, \tag{46}$$

and let  $\bar{\lambda}^{(k)} = \lim_{j \rightarrow \infty} \lambda_j^{(k)}$ . Due to (43) we have

$$\zeta^{(k+1)}(\bar{\lambda}^{(k)}) \geq \zeta^{(k)}(\bar{\lambda}^{(k)}) = \bar{\lambda}^{(k)}. \tag{47}$$

If  $\bar{\lambda}^{(k)}$  is also a fixed-point of  $\zeta^{(k+1)}$  inequality (47) holds as an equality and there is nothing to prove. Assume then that  $\zeta^{(k+1)}(\bar{\lambda}^{(k)}) > \bar{\lambda}^{(k)}$  and consider the sequence  $\lambda_{j+1} = \zeta^{(k+1)}(\lambda_j)$ ,  $j \geq 0$ , with initial guess  $\lambda_0 = \lambda^{(k)}$ . Based on the fact that  $\zeta^{(k+1)}$  increases as  $\lambda$  increases, it follows that  $\lambda_j$  forms a nondecreasing sequence, and therefore  $\{\lambda_j\}$  converges to a fixed-point of  $\zeta^{(k+1)}$ , i.e.,

$$\lim_{j \rightarrow \infty} \lambda_j = \bar{\lambda}^{(k+1)} = \zeta(\bar{\lambda}^{(k+1)})$$

with  $\bar{\lambda}^{(k+1)} \geq \bar{\lambda}^{(k)}$ . Now since after  $N$  steps the subspace  $X_k$  becomes  $\mathbb{C}^N$ , it follows that  $\zeta^{(N)}$  equals  $\zeta$  and so  $\{\bar{\lambda}^{(k)}\}$  must converge to  $\lambda_{\text{GDP}}$  from below in at most  $N$  steps, and the proof concludes.  $\square$

Before we end the section, we emphasize again that for the success of the projection approach, the subspace  $X_k$  must capture information associated with the largest singular values, as occurs, e.g., with the subspace generated by the GKB algorithm at step  $k$ . Of course, as the GKB algorithm proceeds, more and more information associated with the largest singular values of  $\tilde{F}$  is captured [8,22]. As a result, the sequence  $\zeta^{(k)}(\lambda)$  will quickly capture the information of  $\zeta(\lambda)$  for a range of values of  $\lambda$  inside the part of the singular spectrum of  $\tilde{F}$  that is captured by the GKB algorithm in  $k$  steps. This explains the excellent quality of approximation of function  $\vartheta(\lambda)$  by the sequence  $\vartheta^{(k)}(\lambda)$  displayed in Fig. 1. Another property in favor of the GKB algorithm is that the regularized solution and the corresponding residual satisfy property (43) [4, Theorem 2.1]. Finally, we notice that subspaces  $X_k$  that do not guarantee fulfillment of condition (43) can also be used in the projection approach. The difference in this case is that the sequence  $\bar{\lambda}^{(k)}$  is not necessarily monotonic.

5.2. Implementation of LSM based projection approach equipped with GDP: use of GKB algorithm

Recall that application of  $k < n$  GKB steps to  $\tilde{F}$  with initial vector  $r_z / \|r_z\|_2$  yields three matrices: a lower bidiagonal matrix  $B_k \in \mathbb{C}^{(k+1) \times k}$  and two matrices  $U_{k+1} \in \mathbb{C}^{m \times (k+1)}$  and  $V_k \in \mathbb{C}^{n \times k}$  with orthonormal columns, such that

$$\beta_1 U_{k+1} e_1 = \tilde{r}_z = \beta_1 u_1, \tag{48}$$

$$\tilde{F} V_k = U_{k+1} B_k, \tag{49}$$

$$\tilde{F}^H U_{k+1} = V_k B_k^H + \alpha_{k+1} v_{k+1} e_{k+1}^T, \tag{50}$$

where  $e_k$  denotes the  $k$ -th unit vector in  $\mathbb{R}^{k+1}$ . The columns of  $V_k$  provide an orthonormal basis for the generated Krylov subspace  $\mathcal{K}_k(\tilde{F}^H \tilde{F}, \tilde{F}^H \tilde{r}_z)$ , an excellent choice for use when solving ill-posed problems [8,21]. GKB iterations constitute the basis of LSQR method [29,30]. LSQR is designed to construct approximate solutions  $g_z^{(k)}$  to the solution  $g_{LS}$  of the least squares problem

$$g_{LS} = \operatorname{argmin}_{g \in \mathbb{C}^n} \|\tilde{F}g - r_z\|_2^2 \tag{51}$$

defined by  $g_z^{(k)} = V_k y^{(k)}$ , where  $y^{(k)}$  solves the *projected* least squares problem

$$\min_{y \in \mathbb{C}^k} \|B_k y - \beta_1 e_1\|_2. \tag{52}$$

In practical computations  $g_z^{(k)}$  is computed via a QR factorization of  $B_k$  which allows for an efficient updating of the LSQR iterates; the reader is referred to [29] for details.

LSQR is also well suited for solving the “damped least squares problem” (34) for fixed  $\lambda$  [29]. In this case, the  $k$ -th approximate solution is taken to be

$$g_\lambda^{(k)} = V_k y_\lambda^{(k)}, \tag{53}$$

where  $y_\lambda^{(k)}$  solves the regularized projected problem

$$y_\lambda^{(k)} = \operatorname{argmin}_{y \in \mathbb{C}^k} \{ \|B_k y - \beta_1 e_1\|_2^2 + \lambda^2 \|y\|_2^2 \}, \tag{54}$$

which can be handled efficiently using the QR factorization of  $(B_k^T; \lambda I_k)^H$ . On its turn,  $g_\lambda^{(k)}$  can be computed using (53) or through an updating formula which does not require any storage of  $V_k$ , see Paige and Saunders [29]. Note that due to (48) and (49), the residual vector  $r_\lambda^{(k)} = r_z - \tilde{F} g_{\lambda,z}^{(k)}$  and the regularized solution  $g_{\lambda,z}^{(k)}$  satisfy

$$\|r_\lambda^{(k)}\| = \|\beta_1 e_1 - B_k y_\lambda^{(k)}\|, \quad \|g_\lambda^{(k)}\| = \|y_\lambda^{(k)}\|. \tag{55}$$

In addition, if we let the singular value decomposition of  $B_k$  be

$$B_k = P_k \begin{pmatrix} \Sigma_k \\ 0 \end{pmatrix} Q_k^H = \sum_{i=1}^k \sigma_i^{(k)} p_i q_i^T, \tag{56}$$

where  $P_k \in \mathbb{C}^{(k+1) \times (k+1)}$  and  $Q_k \in \mathbb{C}^{k \times k}$  are orthogonal, and  $\Sigma_k = \operatorname{diag}(\sigma_1^{(k)}, \dots, \sigma_k^{(k)})$  with  $\sigma_1^{(k)} \geq \sigma_2^{(k)} \geq \dots \geq \sigma_k^{(k)} > 0$ , then it is immediate to check that

$$\|y_\lambda^{(k)}\|_2^2 = \beta_1^2 \sum_{i=1}^k \frac{[\sigma_i^{(k)}]^2 \xi_{1i}^2}{([\sigma_i^{(k)}]^2 + \lambda^2)^2}, \quad \|r_\lambda^{(k)}\|_2^2 = \beta_1^2 \sum_{i=1}^k \frac{\lambda^4 \xi_{1i}^2}{([\sigma_i^{(k)}]^2 + \lambda^2)^2} + \delta_0^{(k)2} \tag{57}$$

where  $\xi_{1i}$  denotes the  $i$ -th component of the first row of matrix  $P_k$ , and  $\delta_0^{(k)}$  is the 2-norm of the incompatible part of  $\beta_1 e_1$  that lies outside  $\mathcal{R}(B_k)$ . Moreover, analogously to the squared residual norm  $\mathbf{x}(\lambda)$  and the squared solution norm  $\mathbf{y}(\lambda)$ ,  $\|r_\lambda^{(k)}\|_2^2$  increases with  $\lambda$  and  $\|y_\lambda^{(k)}\|_2^2$  decreases.

Thanks to Theorem 5.3 and the approximation properties of the Krylov subspace generated by the GKB algorithm, we can now construct approximations to  $\lambda_{\text{GDP}}$  using a nondecreasing finite sequence of fixed-points  $\bar{\lambda}^{(k)}$  of  $\zeta^{(k)}$ . From the practical point of view, this gives rise to an algorithm for computing  $\lambda_{\text{GDP}}$  and the corresponding regularized solution, which we will refer to as PGDP-FP. The main steps of PGDP-FP can be summarized as follows:

---

**PGDP-FP:**

---

1. Using the GKB algorithm, for a grid point  $\mathbf{z}$  determine an integer  $j$  such that condition (37) is satisfied
  2. Set  $\ell = j$ , compute the fixed-point  $\bar{\lambda}^{(\ell)}$  of  $\zeta^{(\ell)}$  and set  $\lambda_0 = \bar{\lambda}^{(\ell)}$ ,  $\lambda_{\text{old}} = \lambda_0$ ,  $\ell \leftarrow \ell + 1$ .
  3. Perform one more GKB step and compute the fixed-point  $\bar{\lambda}^{(\ell)}$  of  $\zeta^{(\ell)}$  taking  $\lambda_0$  as starting value.  
Set  $\lambda_{\text{old}} = \lambda_0$ ,  $\lambda_0 = \bar{\lambda}^{(\ell)}$ .
  4. **If** stopping criterion is satisfied **do**  
 $\lambda_{\text{GDP}} = \lambda_{\text{old}}$   
**else do**  
 $\ell \leftarrow \ell + 1$   
 Go to step 3.  
**end if**
  5. Compute the regularized solution  $g_{\bar{\lambda}}^{(\ell)}$
- 

For practical purposes, we note that computing fixed-points for each  $\ell$  requires solving the projected problem (54) for several values of  $\lambda$  and for increasing values of  $\ell$ . This can be done following the ideas of the LSQR algorithm at a cost of approximately  $\mathcal{O}(\ell)$  arithmetic operations [30]. Moreover, since very often a fairly small number of steps is required for convergence, the overall cost of PGDP-FP is dominated by  $\ell$  matrix-vector products with  $\tilde{F}$  and  $\tilde{F}^H$  for some moderate number  $\ell$ .

Taking into account the monotonicity of  $\bar{\lambda}^{(\ell)}$ , we choose to stop the outer iterations when the relative change of consecutive fixed-points,

$$\left| \lambda^{(\bar{\ell}+1)} - \bar{\lambda}^{(\ell)} \right| < \epsilon \bar{\lambda}^{(\ell)}, \tag{58}$$

is sufficiently small, where  $\epsilon$  is a tolerance parameter.

Turning to the implementation of LSM for large-scale problems, assume that a grid point  $\mathbf{z} \in D$  is chosen and that the regularization parameter  $\lambda_{\text{GDP}}$  is determined by PGDP-FP. When this is the case, an associated  $\ell$ -dimensional subspace  $X_\ell$  ( $k = \ell + p$ ,  $p \geq 0$ ) is determined which concentrates relevant information of the far-field matrix. Then we can now design a specific method for inverse scattering problems following LSM-PGDP where the approximating subspace  $X_k$  is constructed by performing  $p$  extra GKB steps. For this it suffices to replace steps 1, 2, 3 and 4 of LSM-PGDP by PGDP-FP and then proceed with traditional LSM applied to the projected problem (54) with GDP as parameter choice method. However, a word of caution seems appropriate with regard to the practical implementation of the algorithm when we choose  $p$  equal to or near zero. The reason is that the information captured in  $X_k$  may not be sufficient to guarantee that (37) is satisfied in relation to other grid point  $\mathbf{z}$ , in which case the projected discrepancy

equation (33) may not have any root. A way to overcome this difficulty is by considering a modification of the projected discrepancy equation of the form

$$\widehat{G}^{(k)}(\lambda) = \|\widetilde{F}g_{\lambda,z}^{(k)} - r_z\|_2^2 - \mu_z^{(k)}\lambda^2 - (\delta_F\|g_{\lambda,z}^{(k)}\|_2)^2 = 0, \tag{59}$$

where  $\mu_z^{(k)}$  is the incompatibility measure of the projected far-field equation  $\widetilde{F}_k g = r_z$  defined as

$$\mu_z^{(k)} = \inf_{g \in X_k} \|\widetilde{F}_k g - r_z\|_2. \tag{60}$$

For further information about the incompatibility measure for linear operator equations, the reader is referred to A.G. Yagola [33, Chapter 2, page 29]. As for the incompatibility measure associated to the projected far-field equation, it is immediate to see that  $\mu_z^{(k)}$  equals  $\delta_0^{(k)}$  introduced in Eq. (35) and that  $\widehat{G}^{(k)}(\lambda) = G^{(k)}(\lambda) - \delta_0^{(k)\lambda^2}$ . Additionally, using the singular system of  $\widetilde{F}_k$  and (35) it is not difficult to see that  $\widehat{G}^{(k)}$  always has a unique root  $\bar{\lambda}^{(k)}$  satisfying

$$\sqrt{\delta_F\sigma_k^{(k)}} \leq \bar{\lambda}^{(k)} \leq \sqrt{\delta_F\sigma_1^{(k)}}. \tag{61}$$

Summarizing, in our implementation of LSM-PGDP based on the GKB algorithm, for chosen grid point  $z$  a subspace  $X_k$  is determined following steps 1–4 of PGDP-FP, and then the regularization parameter is computed for the other grid points using the modified discrepancy equation (59) taking advantage of the SVD of the  $(k + 1) \times k$  bidiagonal matrix  $B_k$ , with the observation that this decomposition needs to be computed no more than once.

### 6. Linear sampling method based projection approach equipped with IMPC

As the GDP can fail when the noise level  $\delta_F$  is not accurately estimated, methods that do not rely on this estimate seem favorable. The purpose of this section is to introduce an LSM-based projection approach using IMPC as parameter choice rule. Recall that IMPC selects as regularization parameter the largest local maximizer  $\bar{\lambda}$  of the function  $\Psi(\lambda) = \|r_z - \widetilde{F}g_\lambda\|_2^2\|g_\lambda\|_2^2$  and that this maximizer corresponds to a fixed-point of the function  $\phi(\lambda) = \|r_z - \widetilde{F}g_\lambda\|_2/\|g_\lambda\|_2$ . The following result asserts that this maximizer can be efficiently computed through a fixed-point iteration process with appropriate iteration function.

**Theorem 6.1.** *For fixed  $z$  and  $\lambda > 0$  consider the function  $\xi : \mathbb{R}^+ \mapsto \mathbb{R}^+$  defined by*

$$\xi(\lambda) = \frac{\lambda^2}{\phi(\lambda)}. \tag{62}$$

Then  $\xi$  increases as  $\lambda$  increases and  $\xi(\lambda) \leq \sigma_1$  for all  $\lambda > 0$ . Further, consider the sequence

$$\lambda_{k+1} = \xi(\lambda_k), \quad k \geq 0. \tag{63}$$

Then  $\lambda_k$  converges monotonically to the largest fixed point of  $\xi$  as long as the initial guess  $\lambda_0$  is chosen in the interval  $[\frac{\sqrt{3}}{3}\sigma_1, \sigma_1]$ .

**Proof.** See [5].

Algorithmically, IMPC can be described as follows [5].

---

**Improved version of MPC algorithm (IMPC)**

---

**Input:**  $\sigma_1, tol$

1. Set  $k = 0$  and choose  $\lambda_0$  in the interval  $[\frac{\sqrt{3}}{3}\sigma_1, \sigma_1]$
  2. Compute  $s_0 = \xi(\lambda_0)/\lambda_0$ .
  3. **while** ( $|s_k - 1| > tol$ ) **do**  
 $\lambda_{k+1} = \xi(\lambda_k), s_k = \lambda_{k+1}/\lambda_k$   
 $k = k + 1$   
**end while**
  4. **if** ( $\phi'(\lambda_k) > 1$ ) **do**  
 $\bar{\lambda} = \lambda_k$   
**elseif** ( $\phi'(\lambda_k) = 1$ ) **do**  
Set  $k = 0, \lambda_0 = 0.9 * \lambda_k$ , and go to step 2  
**end if**
- 

We now consider an implementation of IMPC for large-scale problems. To this end, for fixed grid point  $\mathbf{z}$  let  $\xi^{(k)} : \mathbb{R}^+ \mapsto \mathbb{R}^+, k = 1, \dots, N$ , be a sequence of functions defined by

$$\xi^{(k)}(\lambda) = \frac{\lambda^2}{\phi^{(k)}(\lambda)}, \quad \phi^{(k)}(\lambda) = \frac{\|r_{\mathbf{z}} - \tilde{F}_k g_{\lambda, \mathbf{z}}^{(k)}\|_2}{g_{\lambda, \mathbf{z}}^{(k)}}. \tag{64}$$

As before, assume that the far-field matrix  $\tilde{F}$  is nonsingular and that the subspaces  $X_k$  are chosen so that condition (43) holds true. Under these assumptions it follows that  $\Psi(\lambda)$  has at least a maximum, which we denote by  $\bar{\lambda}$ , and that

$$\xi(\lambda) = \xi^N(\lambda) \geq \xi^{N-1}(\lambda) \geq \dots \geq \xi^1(\lambda). \tag{65}$$

Based on both this result and the assumption that  $\xi^{(k)}$  has a fixed point  $\bar{\lambda}^{(k)}$  for some integer  $k \geq 1$ , we can follow the line of analysis of the proof of Theorem 5.3 to prove that  $\bar{\lambda}^{(k)}$  converges to the largest maximizer  $\bar{\lambda}$  of  $\Psi$  as  $k \rightarrow N$ .

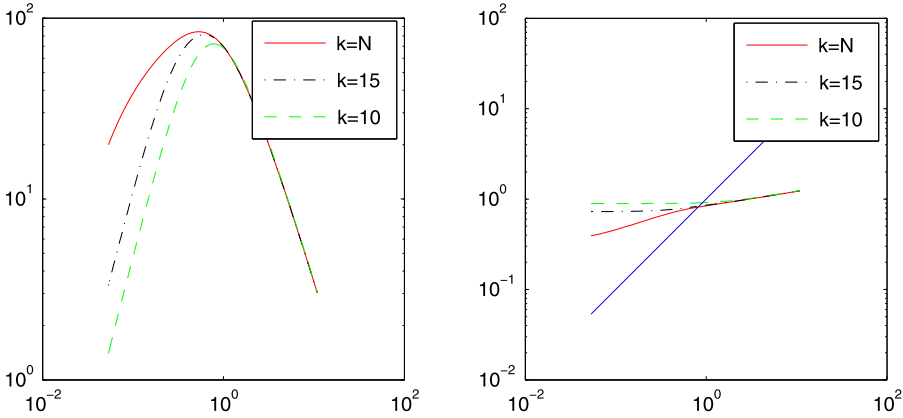


Fig. 3. Functions  $\widehat{\Psi}^{(k)}$  (left) and  $\widehat{\xi}^{(k)}$  (right) for some values of  $k$ . The data correspond to a far-field equation with far-field matrix  $\widetilde{F}$  of size  $512 \times 512$  and relative noise level 1%.

6.1. Implementation of LSM based projection approach equipped with IMPC: use of GKB algorithm

Similarly to the sequence of approximations to  $\lambda_{\text{GDP}}$ , the quality of the approximation of  $\bar{\lambda}^{(k)}$  to  $\bar{\lambda}$  will depend on how many dominant singular values of  $\widetilde{F}$  are captured by  $\widetilde{F}_k$ ; this motivates again the choice of the subspace generated by the GKB algorithm. Thus, the only issue that requires discussion is under what condition the function  $\xi^{(k)}$  has nonzero fixed-points. The difficulty here is that, as  $\phi^{(k)}(0) > 0$  due to (57) and  $\phi^{(k)}(\lambda) > \lambda$  for  $\lambda > \sigma_1(B_k)$  due to [2, Lemma 1], the question about existence of fixed-points of  $\phi^{(k)}$  (hence of  $\xi^{(k)}$ ) remains without definite answer. The key idea to circumvent this difficulty is to consider AR, like the case of the projected discrepancy equation, a modification of the iteration function  $\xi^{(k)}$ , involving the incompatibility measure  $\mu_z^{(k)}$  and defined by

$$\widehat{\xi}^{(k)}(\lambda) = \frac{\lambda^2}{\widehat{\phi}^{(k)}(\lambda)}, \quad \widehat{\phi}^{(k)}(\lambda) = \frac{\sqrt{\|\widetilde{F}g_{\lambda,z}^{(k)} - r_z\|^2 - \mu_z^{(k)2}}}{\|g_{\lambda,z}\|}. \tag{66}$$

Since the squared incompatibility measure is subtracted from the squared residual norm, because of (57) we have that  $\widehat{\phi}^{(k)}(0) = 0$ . From this result together with the fact that  $\widehat{\phi}^{(k)}(\lambda) > \lambda$  for  $\lambda > \sigma_1(B_k)$ , which follows from [2, Lemma 1], we conclude that  $\widehat{\phi}^{(k)}$  always has a fixed point (which is also fixed-point of  $\widehat{\xi}^{(k)}$ ) that maximizes a related function  $\widehat{\Psi}^{(k)}$  defined in obvious way and can be used to approximate the maximizer  $\bar{\lambda}$  of  $\Psi$ . Obviously, as the incompatibility measure vanishes for  $k = N$ , the sequence of fixed-points computed in this way has to converge to  $\bar{\lambda}$ . For illustration purposes, a few functions  $\widehat{\Psi}^{(k)}$  and corresponding iterations functions  $\widehat{\xi}^{(k)}$  are displayed in Fig. 3.

Again, the remarkable closeness between  $\widehat{\Psi}^{(k)}(\lambda)$  and  $\Psi(\lambda)$  for a large range of values of  $\lambda$  approaching the maximizer  $\bar{\lambda}$  displayed in this figure is because of the approximation

properties of the Krylov subspace generated by the GKB algorithm. A similar comment applies for the fixed-points of functions  $\widehat{\xi}^{(k)}$  when compared to the one of  $\xi$ .

Having shown that the maximizer of  $\Psi$  can be approximated through a sequence of fixed-points of  $\widehat{\xi}^{(k)}$ , we can now describe our projection approach for determining the regularization parameter chosen by IMPC, which we will denote by PIMPC-FP.

---

**PIMPC-FP:**

---

1. For fixed grid point  $\mathbf{z}$  apply  $q$  GKB steps to  $\widetilde{F}$  with starting vector  $u_1 = r_{\mathbf{z}}/\|r_{\mathbf{z}}\|$ .
  2. Set  $\ell = q$ , compute the fixed-point  $\bar{\lambda}^{(\ell)}$  of  $\widehat{\xi}^{(\ell)}$  and set  $\lambda_0 = \bar{\lambda}^{(\ell)}$ ,  $\lambda_{\text{old}} = \lambda_0$ ,  $\ell \leftarrow \ell + 1$ .
  3. Perform one more GKB step and compute the fixed-point  $\bar{\lambda}^{(\ell)}$  of  $\widehat{\xi}^{(\ell)}$  taking  $\lambda_0$  as starting value. Set  $\lambda_{\text{old}} = \lambda_0$ ,  $\lambda_0 = \bar{\lambda}^{(\ell)}$ .
  4. **If** stopping criterion is satisfied **do**  
 $\bar{\lambda} = \lambda_{\text{old}}$   
**else do**  
 $\ell \leftarrow \ell + 1$   
 Go to step **3**.  
**end if**
  5. Compute the regularized solution  $g_{\bar{\lambda}}^{(\ell)}$
- 

We now turn to an implementation of LSM for large-scale inverse scattering problems based on the GKB algorithm and IMPC as root finder. Assume that for  $\mathbf{z} \in D$  the regularization parameter  $\bar{\lambda}$  chosen by IMPC is determined through PIMPC-FP. Then an associated  $\ell$ -dimensional subspace  $X_\ell$  is determined which concentrates relevant information of the far-field matrix. Our new method for large-scale inverse scattering problems follows LSM-PGDP where the approximating subspace  $X_k$ ,  $k = \ell + p$ ,  $p \geq 0$ , is constructed by performing  $p$  additional GKB steps. To this end, it suffices to replace steps 1, 2, 3 and 4 of LSM-PGDP by PIMPC-FP and then proceed with traditional LSM applied to the projected problem (54) with IMPC as parameter choice method.

**7. Kirsch’s method based projection approach**

The discussions and approaches described before can now be used as a starting point for an implementation of Kirsch’s method for the reconstruction of 3D object that exhibit large-scale far-field matrices. We first note that in the finite dimensional framework the regularized solution for Kirsch’s method is

$$g_{\lambda, \mathbf{z}} = \operatorname{argmin}_{g \in \mathbb{C}^n} \{ \|\widetilde{A}^{1/4}g - r_{\mathbf{z}}\|_2^2 + \lambda^2 \|g\|_2^2 \} \tag{67}$$

where  $\tilde{A} = (\tilde{F}_q^H \tilde{F}_q)$ . The choice of  $\lambda$  has been done via Morozov’s generalized discrepancy principle (GDP) [1,3,24] and more recently via MPC [7]. For the projection approach we require the solution to the projected regularized problem given by

$$g_{\lambda,z}^{(k)} = \operatorname{argmin}_{g \in X_k} \left\{ \|\tilde{A}_k g - r_z\|^2 + \lambda^2 \|g\|^2 \right\} \tag{68}$$

in which  $\tilde{A}_k = \tilde{A}^{1/4} P_k$ , with  $P_k$  being the orthogonal projector onto appropriate subspace  $X_k$ . Thus, all we need is to solve efficiently this projected problem and then proceed as in the traditional LSM based projection approach described in previous sections. For instance, if the regularization parameter is chosen by GDP, then the discrepancy equation reads

$$\check{G}(\lambda) \doteq \{ \|\tilde{A}^{1/4} g_{\lambda,z} - r_z\|_2^2 - (\delta_A \|g_{\lambda,z}\|_2)^2 \} \tag{69}$$

where  $\delta_A$  is a noise estimate such that  $\|(F^H F)^{1/4} - (\tilde{F}^H \tilde{F})^{1/4}\|_2 \leq \delta_A$ , and we have to consider the corresponding “projected discrepancy equation”

$$\check{G}^{(k)}(\lambda) = \|\tilde{A}^{1/4} g_{\lambda,z}^{(k)} - r_z\|_2^2 - (\delta_A \|g_{\lambda,z}^{(k)}\|_2)^2 = 0, \tag{70}$$

where  $g_{\lambda,z}^{(k)}$  solves the regularized projected problem (68). A similar procedure should be followed if the regularization parameter is chosen by IMPC.

However, despite the simplicity of the above description, we emphasize that solving the regularized projected problem (68) is not as simple as one could wish. The major problem here is that to determine  $g_{\lambda,z}^{(k)}$ , the product of a matrix function and a vector,  $f(A)b$ , needs to be computed, for Hermitian  $A$  and  $f(t) = t^{1/4}$ ,  $t \in \mathbb{R}^+$ . Such a computation is not always straightforward for large  $A$ . A survey of methods for approximating matrix functions can be found in Higham’s book [23, Chapter 13]. Our approach follows the well-known Lanczos approximation to  $f(\tilde{A})b$  based on the decomposition

$$\tilde{A}V_k = V_k \tilde{T}_k + \beta_k v_{k+1} e_k^T, \tag{71}$$

where the columns of  $V_k = [v_1, v_2, \dots, v_k]$  form an orthonormal basis of the Krylov subspace  $\mathcal{K} = \operatorname{span}\{b, \tilde{A}b, \dots, \tilde{A}^{k-1}b\}$  with  $v_1 = b/\|b\|_2$ ,

$$\tilde{T}_k = \begin{bmatrix} \alpha_1 & \beta_1 & & & \\ \beta_1 & \alpha_2 & \beta_2 & & \\ & \ddots & \ddots & \ddots & \\ & & & & \\ & & & b_{k-2} & \alpha_{k-1} & \beta_{k-1} \\ & & & & \beta_{k-1} & \alpha_k \end{bmatrix} \tag{72}$$

and  $e_k \in \mathbb{R}^k$  denotes the  $k$ -th unit canonical vector. Then the Lanczos approximation to  $f(\tilde{A})b$  reads

$$f(\tilde{A})b \approx V_k f(\tilde{T}_k) V_k^H b. \tag{73}$$

Since  $T_k$  is Hermitian and  $k$  is expected to be small,  $f(T_k)$  can be computed efficiently using an eigendecomposition of  $\tilde{T}_k$ . In addition, multiplying both sides of (71) with  $V_k^H$  we obtain  $V_k^H \tilde{A} V_k = \tilde{T}_k$ . Thus, to solve the regularized projection problem we use the approximation

$$V_k^H f(\tilde{A}) V_k \approx f(\tilde{T}_k). \tag{74}$$

Approximations (73)–(74) imply that we can obtain approximations to the regularized solution for the projected problem (68) defined by

$$g_{\lambda, z}^{(k)} = V_k y_{\lambda}^{(k)}, \quad y_{\lambda}^{(k)} = \left( \tilde{T}^{1/2} + \lambda^2 I_k \right)^{-1} \tilde{T}^{1/4} V_k^H r_z. \tag{75}$$

We now make the crucial observation that, since the solution to the projected problems involves the projection matrix  $\tilde{T}_k$  which is not singular, the incompatibility measure of the projected problem vanishes. Consequently, the projected discrepancy equation will always have a unique root (under mild conditions). Similarly, the iteration function  $\zeta^{(k)}$  on which IMPC is based will always have a fixed point that can be used to approximate the sought regularization parameter. Based on this, the choice of the subspace  $X_k$  can be made following the same steps as PIMPC-FP, with the obvious replacement of GKB algorithm by the Lanczos algorithm.

### 8. Numerical examples

We shall now illustrate the effectiveness of the projection based approaches by presenting numerical results on reconstructions of five surfaces taken from [1, Section 4]. Our examples include an acorn-shaped surface, a cushion-shaped surface, an ellipsoid, a peanut-shaped surface, and a unit sphere. To simulate relatively large perturbed data, all examples use  $1026 \times 1026$  noisy far-field matrices

$$\tilde{F} = F + \epsilon \|F\| \mathcal{N},$$

where  $F$  is a synthetic “noise-free” far-field matrix,  $\mathcal{N}$  is a noise complex matrix normalized such that  $\|\mathcal{N}\|_2 = 1$  with real and imaginary parts being Gaussian, and  $\epsilon$  is an error parameter. For the numerical procedure used to generate synthetic far-field data, the reader is referred to [1, Section 4]. In the appendix we provide a way to estimate the noise level, say  $\delta$  and  $\delta_k$ , based on raw data for the linear sampling method (11) and the factorization method (15) respectively. For the reconstruction we consider a uniform grid in a cube  $[-t, t] \times [-t, t] \times [-t, t]$ ,  $t > 0$ , containing the object, with  $N$  points in

each direction, and denote by  $\mathcal{Z}$  the set of all these grid points. In our numerical reconstructions we use  $t = 1.5$ ,  $N = 55$ , wavenumbers  $k_e = 2$ ,  $k_i = 1$ , and error parameters  $\epsilon = 0.01$  (relative noise level 1%) and  $\epsilon = 0.1$  (relative noise level 10%). As discussed before  $\|g_{\lambda, \mathbf{z}}\|$  becomes arbitrarily large when  $\mathbf{z}$  approaches the boundary from inside and remains large when  $\mathbf{z}$  is outside. Based on the behavior of  $\|g_{\lambda, \mathbf{z}}\|$ , the identification of the object can be made by using the indicator function

$$\mathbf{z} \mapsto W_\lambda(\mathbf{z}) = 1/\|g_{\lambda, \mathbf{z}}\|^2 \tag{76}$$

where  $\lambda$  is a chosen regularization parameter. Alternatively, as  $\|g_{\lambda, \mathbf{z}}\|$  decreases with  $\lambda$ , the identification of the object can also be made by using the indicator function

$$\mathbf{z} \mapsto \lambda(\mathbf{z}) \tag{77}$$

which is expected to behave qualitatively like  $W_\lambda(\mathbf{z})$ . Indeed, if the regularization parameter is chosen by a regularization method such as GDP, due to the convergence properties of GDP and the monotonic behavior of  $\|g_{\lambda, \mathbf{z}}\|$ , large values of  $W_\lambda(\mathbf{z})$  correspond to large values of  $\lambda(\mathbf{z})$  and vice versa. Hence, both  $W_\lambda(\mathbf{z})$  and  $\lambda(\mathbf{z})$  should behave qualitatively like  $W(\mathbf{z}) = 1/\|g_{\mathbf{z}}\|^2$  where  $g_{\mathbf{z}}$  is the unique solution of  $(F^H F)^{1/4} g = r_{\mathbf{z}}$ . The reconstruction is then visualized by plotting the isosurface

$$\mathcal{S} = \{\mathbf{z} \in \mathcal{Z} \mid W_\lambda(\mathbf{z}) = \tau \text{ (resp. } \lambda(\mathbf{z}) = \tau)\},$$

for an isovalue parameter  $\tau$  such that the level set  $\mathcal{S}$  is a suitable visual representation of the unknown object. The isovalue parameter must satisfy  $\min_{\mathbf{z} \in \mathcal{Z}} [W_\lambda(\mathbf{z})] < \tau < \max_{\mathbf{z} \in \mathcal{Z}} [W_\lambda(\mathbf{z})]$  (resp.  $\min_{\mathbf{z} \in \mathcal{Z}} [\lambda(\mathbf{z})] < \tau < \max_{\mathbf{z} \in \mathcal{Z}} [\lambda(\mathbf{z})]$ ), and can be selected by trial and error or based on heuristics, always looking for a representative of the higher values of  $W_\lambda(\mathbf{z})$  (resp.  $\lambda(\mathbf{z})$ ).

As for the choice of the isovalue parameter in practice, a value that has been found to yield good reconstructions is one near the mean value of the indicator function due to Fares et al. [17], referred to as the global mean and standard deviation (GMSD) heuristic and defined as

$$\tau = \text{mean}_{\mathbf{z} \in \mathcal{Z}} [I(\mathbf{z})] + 2\text{std}_{\mathbf{z} \in \mathcal{Z}} [I(\mathbf{z})], \tag{78}$$

where  $I(\mathbf{z})$  stands for any of the indicator functions (76) or (77).

To illustrate the role of the isovalue parameter  $\tau$  in the reconstructions, we consider the problem of reconstructing the acorn-shaped surface from data with relative noise level 1% by using Kirsch’s method equipped with GDP. For this we compute the indicator function  $W_\lambda(\mathbf{z})$  associated with the large and projected problem, respectively, as well as the indicator function  $W(\mathbf{z})$  corresponding to the noise-free case.

Fig. 4 shows unidimensional views of  $W(\mathbf{z})$ ,  $W_\lambda(\mathbf{z})$ , the corresponding isovalue parameters displayed as horizontal lines, and the reconstructions. Unidimensional versions of the indicator function are obtained by stacking the columns of the matrix

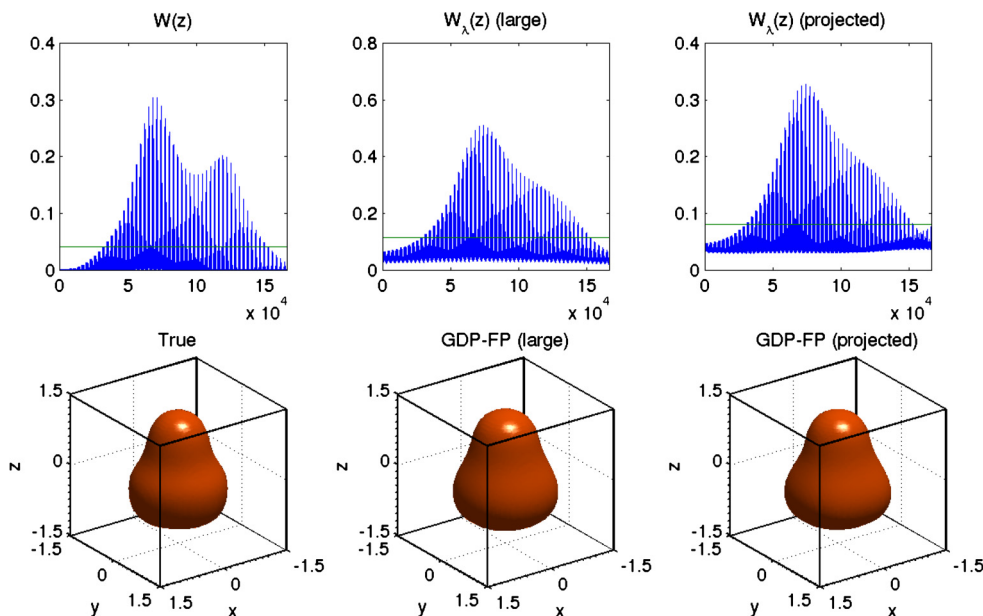


Fig. 4. Top: unidimensional version of  $W(z)$  and  $W_\lambda(z)$  for Kirsch’s method equipped with GDP. Bottom: reconstructed objects from far-field matrix with relative noise level 1%.

$I(z = (x_1, x_2, x_3))$  for fixed  $x_3$  but varying on the mesh. As we can observe, not only the indicator functions behave similarly but also the reconstructions look very good. For the reconstructions, the isovalue parameters were selected so that the reconstructed objects have approximately the same aspect ratio, taking as starting values those parameters defined in (78). For the projected approach we selected  $k = 30$ . The same trend is observed when the subspace is determined automatically as described at the end of the previous section.

Fig. 5 shows unidimensional views of  $W(z)$ ,  $\lambda(z)$ , the corresponding isovalue parameters displayed as horizontal lines, and the reconstructions. Again, we use Kirsch’s method equipped with GDP and select a Krylov subspace of dimension  $k = 30$ . As before, we observe that the indicator functions look very similar. We also observe that the reconstructions suffer some deformation but the shape of the objects is apparent.

We now illustrate the role of the isovalue parameter  $\tau$  in the reconstructions using Kirsch’s method and traditional LSM, all equipped with IMPC, the projection approach being implemented with a Krylov subspace of dimension  $k = 30$ . Fig. 6 shows the indicator function  $\lambda(z)$  for three cases: the first case considers Kirsch’s method applied to the large problem, the second case considers the Kirsch based projection approach, and the third case considers the LSM based projection approach. As we can observe, the reconstructions obtained with Kirsch’s method look very similar and of good quality whereas the quality of the reconstruction obtained with traditional LSM is degraded. This is partially justified by the fact that the indicator function for LSM looks somewhat

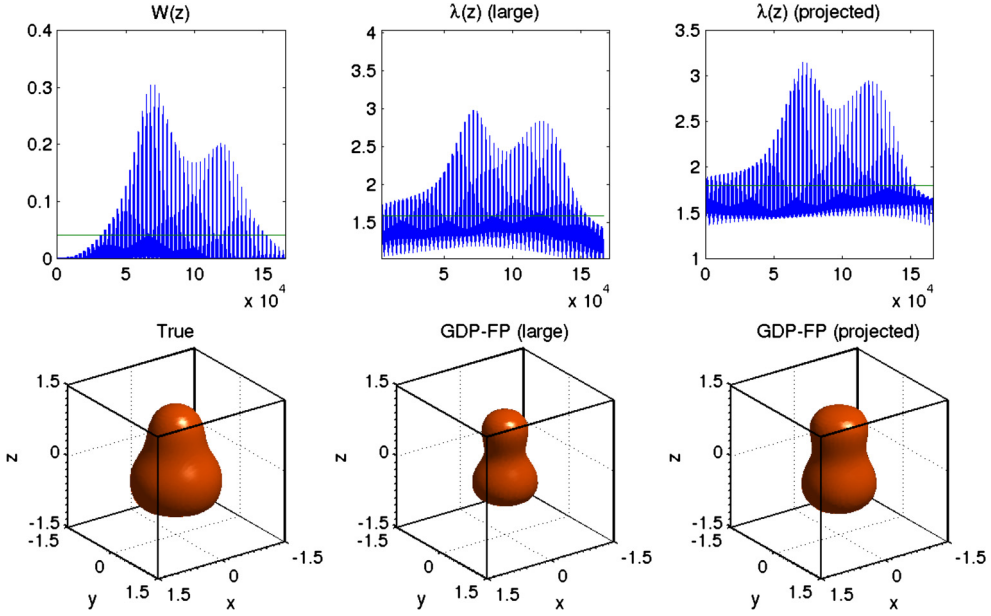


Fig. 5. Top: unidimensional version of  $W(\mathbf{z})$  and  $\lambda(\mathbf{z})$  for Kirsch’s method equipped with GDP. Bottom: reconstructed objects from far-field matrix with relative noise level 1%.

different compared to the indicator functions for Kirsch’s method. Notice also that the range of  $\lambda(\mathbf{z})$  for traditional LSM differs significantly from the range of  $\lambda(\mathbf{z})$  for Kirsch’s method. The reason is that for LSM we have  $\sigma_{\min}(\tilde{F}) < \lambda(\mathbf{z}) < \sigma_{\max}(\tilde{F})$ , while for Kirsch’s method  $\sigma_{\min}^{1/2}(\tilde{F}) < \lambda(\mathbf{z}) < \sigma_{\max}^{1/2}(\tilde{F})$ .

We shall now illustrate the effectiveness of the projection approach when applied to the other surfaces, concentrating on Kirsch’s method only as it performed better than traditional LSM. For the reader’s sake we find instructive to report the convergence speed of the projection approach compared to conventional implementations of GDP or IMPC. To this end we consider Kirsch’s method equipped with GDP and IMPC respectively, using far-field data with noise level 1% and Krylov subspaces of dimension  $k = 30$ . Table 1 displays the time spent by three versions for GDP and two versions for IMPC. In this table, (LP) and (PP) refer to large and projected problem, respectively. Thus GDP-FP (LP) indicates application of GDP-FP to large problems, GDP-FP (PP) indicates application of GDP-FP to projected problems, and so on. In addition, GDP-D refers to an implementation of GDP based on Dekker’s algorithm as root finder (available as `fzero.m` in Matlab). The results show that the projection approach gets faster than the non-projected one by a factor ranging between 25 to 30. They also confirm previous evidence that the fixed point approach outperforms other root finders such as regula falsi method when applied to the discrepancy equation, as reported in [5]. For completeness, we also observe that when the subspace dimension is determined automatically, for GDP-FP (PP) the dimension ranges from 22 to 24, whereas for IMPC-FP (PP) the dimension ranges from 30 to 32.

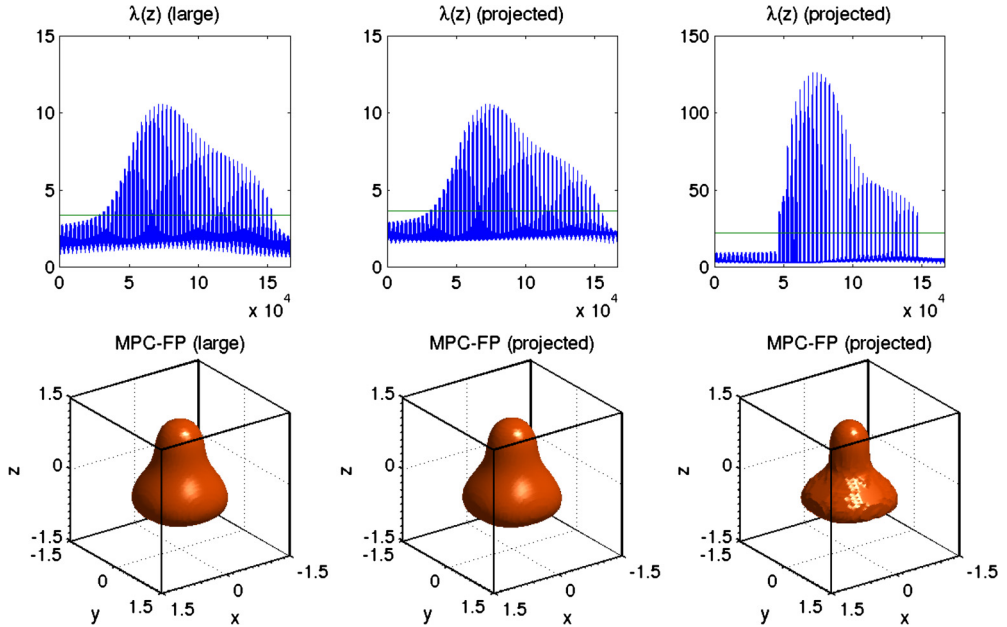


Fig. 6. Top: unidimensional view of  $\lambda(z)$  for Kirsch’s method and traditional LSM equipped with IMPC. Bottom: reconstructions from far-field data with relative noise level 1%. Figures on first and second columns correspond to Kirsch’s method. Figures on third column correspond to traditional LSM.

Table 1  
CPU time in seconds for several versions of Kirsch’s method.

	Acorn	Cushion	Ellipsoid	Peanut	Sphere
GDP-D (LP)	934.51	955.17	789.41	804.74	792.85
GDP-FP (LP)	524.95	540.85	521.35	512.96	522.58
IMPC-FP (LP)	549.68	536.89	557.77	528.37	532.84
GDP-FP (PP)	30.17	30.28	29.77	32.61	30.45
IMPC-FP (PP)	36.98	36.01	38.32	37.89	37.80

We now proceed by describing other reconstructions obtained with Kirsch’s method based projection approach equipped with GDP and IMPC. As before, we consider far-field data with noise level 1% and choose  $k = 30$  as dimension of the Krylov subspace. The isovalue parameters are chosen by adjusting those obtained by GMSD so that the reconstruction ratio becomes approximately the same. Results are displayed in Fig. 7.

As it appears evident, except for the peanut-shaped surface, the reconstructions look quite good and of similar quality as those obtained for the acorn-shaped surface. Reconstructions obtained with automatic identification of the Krylov subspace did not alter significantly the quality of the reconstructions and are therefore not reported here.

Reconstructions of the five surfaces from far-field data with noise level 10% are displayed in Fig. 8. We notice that the reconstruction quality deteriorates slightly but the pattern of the objects remains informative.

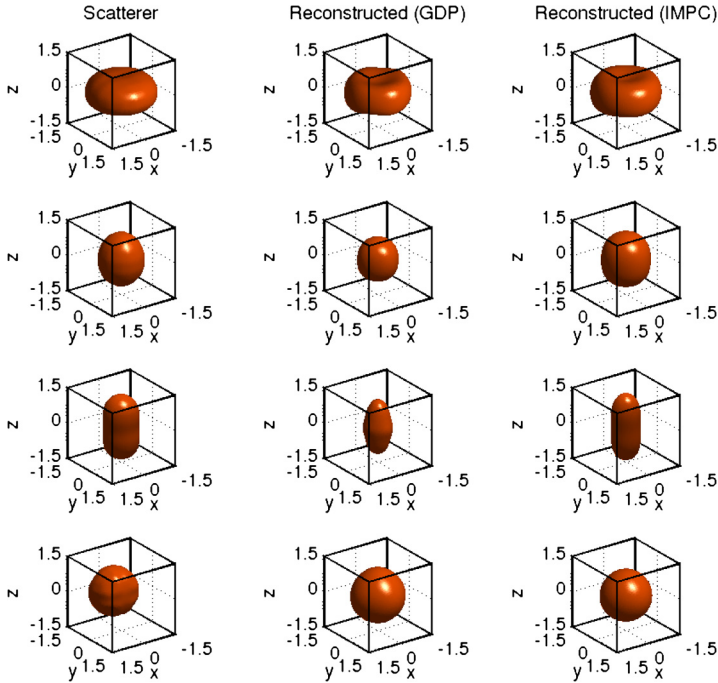


**Fig. 7.** True and reconstructed objects by using Kirsch's based projection approach from far-field matrix of size  $1026 \times 1026$  with relative noise level 1%.

Finally, in order to illustrate our projections methods in a highly contaminated environment, in Fig. 9 we report reconstructions of the acorn-shaped surface from far-field data with noise level 20%. Again, we use Kirsch's method equipped with both GDP and IMPC and project onto a Krylov subspace of dimension  $k = 30$ . In this case, despite the significant deterioration of the reconstructions, we note that both GDP and IMPC are still able to identify the presence of the object.

## 9. Conclusions

We have developed sampling based projection methods for the reconstruction of 3D acoustically penetrable objects that exhibit large-scale far-field matrices. Two classes of methods are considered: methods that exploit knowledge of noise level estimates and methods that do not exploit such information. Regardless of whether the noise level is available or not, the methods rely on the fact that the indicator function used in the reconstructions can be computed efficiently based on Tikhonov regularized solutions involving a small number of variables, thereby reducing significantly the huge amount of calculations required by traditional implementations of linear sampling methods for large problems. Numerical results show that the methods are capable of providing satisfactory visualization of the scatterers at an extremely modest cost. Future work includes

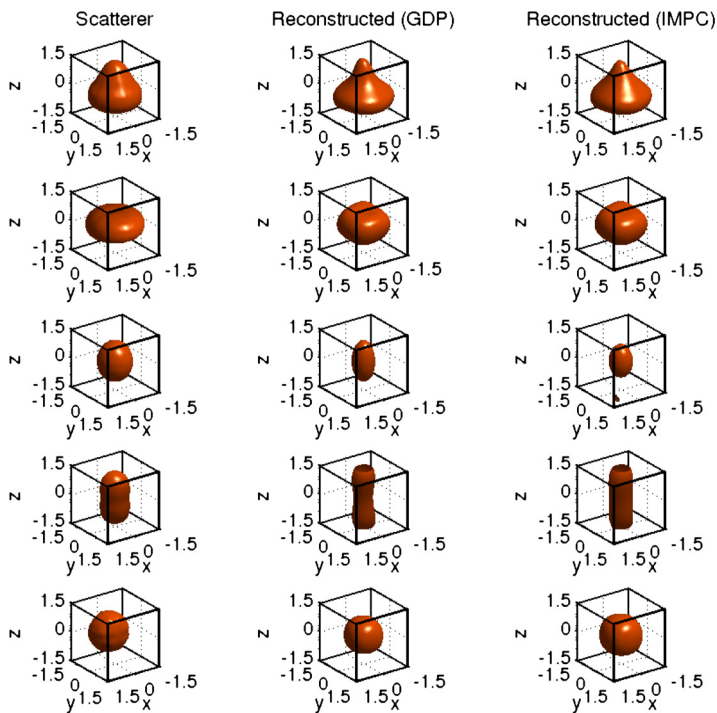


Fig. 8. True and reconstructed objects by using Kirsch’s based projection approach from far-field matrix of size  $1026 \times 1026$  with relative noise level 10%.

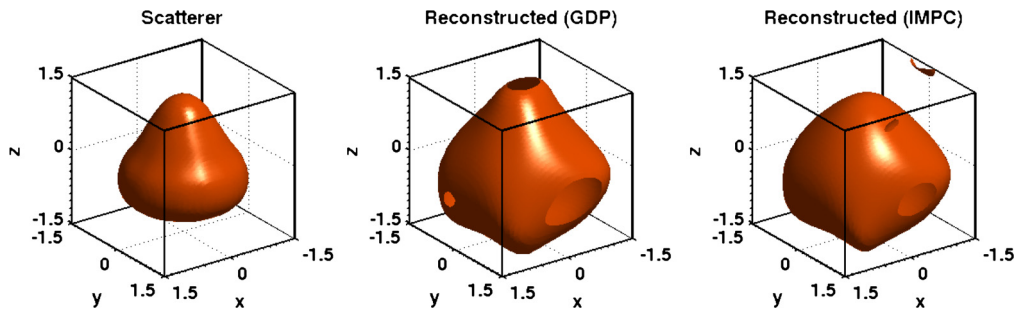


Fig. 9. True and reconstructed objects by using Kirsch’s based projection approach from far-field matrix of size  $1026 \times 1026$  with relative noise level 20%.

exhaustive testing of the methods with larger problems to assess their effective potential.

**Acknowledgement**

The work of the first author is supported by CNPq, Brazil, Grants 308709/2011-0, 477093/2011-6.

**Appendix A**

Let the exact and perturbed far-field matrices be denoted by  $F$  and  $\tilde{F}$ , respectively. The goal is to derive an estimate for  $\|(\tilde{F}^H \tilde{F})^{1/4} - (F^H F)^{1/4}\|_2$  based on raw data  $\tilde{F} = F + E$ . Consider the following definitions:

- a)  $\tilde{D} = \tilde{F}^H \tilde{F} - \tilde{F} \tilde{F}^H, D = F^H F - F F^H,$
- b)  $\tilde{\Delta} = \|\tilde{D}\|_2, \Delta = \|D\|_2,$
- c)  $\mu = \|\tilde{F}\|_2 = \|\tilde{F}^H\|_2, \delta = \|\tilde{F} - F\|_2.$

We start by estimating the error norm  $\delta = \|\tilde{F} - F\|_2$  as follows. Using definitions of  $\tilde{D}$  and  $D$  we have

$$\begin{aligned} \tilde{D} &= \tilde{F}^H \tilde{F} - \tilde{F} \tilde{F}^H - D + D \\ &= \tilde{F}^H \tilde{F} - \tilde{F} \tilde{F}^H - F^H F + F F^H + D \\ &= (\tilde{F}^H \tilde{F} - \tilde{F}^H F) - \tilde{F} \tilde{F}^H + (\tilde{F}^H F - F^H F) + F F^H + D \\ &= \tilde{F}^H (\tilde{F} - F) + (\tilde{F}^H - F^H) F + F F^H - \tilde{F} \tilde{F}^H + D. \end{aligned} \tag{79}$$

Adding

$$(\tilde{F}^H - F^H) \tilde{F} + \tilde{F} F^H + (F - \tilde{F}) \tilde{F}^H$$

on the right hand side of (79) and then subtracting the same quantity, after rearranging terms we have

$$\begin{aligned} \tilde{D} &= \tilde{F}^H (\tilde{F} - F) + (\tilde{F}^H - F^H) (F - \tilde{F}) + (F - \tilde{F}) (\tilde{F}^H - F^H) + (\tilde{F}^H - F^H) \tilde{F} + \\ &\quad (F - \tilde{F}) \tilde{F}^H + \tilde{F} (F^H - \tilde{F}^H) + D \end{aligned}$$

By taking 2-norms we have

$$\tilde{\Delta} \leq \mu \delta + 2\delta^2 + \delta \mu + \delta \mu + \delta \mu + \Delta = 2\delta^2 + 4\mu \delta + \Delta$$

or

$$\delta^2 + 2\mu \delta - \frac{\tilde{\Delta} - \Delta}{2} \geq 0.$$

Solving the inequality for  $\delta$  we get

$$\delta \geq \sqrt{\mu^2 + \frac{\tilde{\Delta} - \Delta}{2}} - \mu. \tag{80}$$

Assuming that  $F$  is near normal, which means  $\Delta \approx 0$ , our first estimate for  $\delta$  based on raw data is taken as

$$\delta_1 = \sqrt{\mu^2 + \frac{\tilde{\Delta}}{2}} - \mu. \tag{81}$$

Since  $\delta_1$  is close to the lower bound of (80) and since for GDP to work we require an upper bound on  $\delta$ , a second estimate can be taken as

$$\delta_2 = \sqrt{\frac{\tilde{\Delta}}{2}}. \tag{82}$$

Obviously  $\delta_2 \approx \delta_1$  only when  $\tilde{F}$  is near normal, i.e, when  $\tilde{\Delta}$  is small, otherwise  $\delta_2 \gg \delta_1$ . Better results are obtained with the choice  $\delta = (\delta_1 + \delta_2)/2$ .

We now derive an estimate for  $\|(\tilde{F}^H \tilde{F})^{1/4} - (F^H F)^{1/4}\|_2$ . Let the SVDs of  $\tilde{F}$  and  $F$  be

$$\tilde{F} = \tilde{U} \tilde{\Sigma} \tilde{V}^H, \quad F = U \Sigma V^H,$$

Setting  $\tilde{B} = \tilde{F}^H \tilde{F}$ ,  $B = F^H F$ , using the above SVDs we have

$$\tilde{B}^{1/4} - B^{1/4} = \tilde{V} \tilde{\Sigma}^{1/2} \tilde{V}^H - V \Sigma^{1/2} V^H = \tilde{C}^H \tilde{C} - C^H C,$$

where  $\tilde{C} = \tilde{\Sigma}^{1/4} \tilde{V}^H$  is a non-normal matrix which can be computed from far-field data, and  $C = \Sigma^{1/4} V^H$ . Hence

$$\tilde{B}^{1/4} - B^{1/4} = \tilde{C}^H \tilde{C} - C^H C = \tilde{C}^H (\tilde{C} - C) + (\tilde{C}^H - C^H) C. \tag{83}$$

Taking norms we have

$$\|\tilde{B}^{1/4} - B^{1/4}\|_2 \leq (\|\tilde{C}\|_2 + \|C\|_2)^H \|\tilde{C} - C\|_2 \tag{84}$$

and the error norm  $\|\tilde{C} - C\|_2$  can be estimated as in the previous case based on the departure from normality of  $\tilde{C}$  and the corresponding matrix norm  $\|\tilde{C}\|_2$ . More precisely, from (81) and (82) we can obtain estimates  $\hat{\delta}_1$  and  $\hat{\delta}_2$  for  $\|\tilde{C} - C\|_2$  as follows

$$\hat{\delta}_1 = \sqrt{\|\tilde{C}\|_2^2 + \frac{\|\tilde{C}^H \tilde{C} - \tilde{C} \tilde{C}^H\|_2}{2}} - \|\tilde{C}\|_2 \tag{85}$$

and

$$\hat{\delta}_2 = \sqrt{\frac{\|\tilde{C}^H \tilde{C} - C \tilde{C}^H\|_2}{2}}. \tag{86}$$

Since  $\|\tilde{C}\|_2 = \tilde{\sigma}_1^{1/4}$ , assuming that  $\sigma_1 \leq \tilde{\sigma}_1$ , the error norm required by Kirsch's method,  $\delta_K \doteq \|\tilde{B}^{1/4} - B^{1/4}\|_2$ , can be estimated from (84) as

$$\delta_K = 2\tilde{\sigma}_1^{1/4}\delta_C, \quad (87)$$

where  $\delta_C$  is either  $\hat{\delta}_1$  or  $\hat{\delta}_2$ . Better results are obtained with the choice  $\delta_C = \hat{\delta}_1$ .

## References

- [1] K. Anagnostopoulos, A. Charalambopoulos, A. Kleefeld, The factorization method for the acoustic transmission problem, *Inverse Probl.* 29 (2013) 1–29.
- [2] F.S.V. Bazán, Fixed-point iterations in determining the Tikhonov regularization parameter, *Inverse Probl.* 24 (2008) 1–15.
- [3] F.S.V. Bazán, Simple and efficient determination of the Tikhonov regularization parameter chosen by the generalized discrepancy principle for discrete-ill-posed problems, *J. Sci. Comput.* 63 (2015) 163–184.
- [4] F.S.V. Bazán, L.S. Borges, GKB-FP: an algorithm for large-scale discrete ill-posed problems, *BIT* 50 (2010) 481–507.
- [5] F.S.V. Bazán, J.B. Francisco, K.H. Leem, G. Pelekanos, Using the linear sampling method and an improved maximum product criterion for the solution of the electromagnetic inverse medium problem, *J. Comput. Appl. Math.* 273 (2015) 61–75.
- [6] F.S.V. Bazán, M.C. Cunha, L.S. Borges, Extension of GKB-FP to large-scale general-form Tikhonov regularization, *Numer. Linear Algebra Appl.* 21 (2014) 316–339.
- [7] F.S.V. Bazán, J.B. Francisco, K.H. Leem, G. Pelekanos, A maximum product criterion as a Tikhonov parameter choice rule for Kirsch's factorization method, *J. Comput. Appl. Math.* 236 (2012) 4264–4275.
- [8] Å. Björck, A bidiagonalization algorithm for solving ill-posed systems of linear equations, *BIT* 28 (1988) 659–670.
- [9] D. Colton, H. Haddar, P. Monk, The linear sampling method for solving the electromagnetic inverse scattering problem, *SIAM J. Sci. Comput.* 24 (2003) 719–731.
- [10] D. Colton, H. Haddar, M. Piana, The linear sampling method in inverse electromagnetic scattering theory, *Inverse Probl.* 19 (2003) 105–137.
- [11] D. Colton, A. Kirsch, A simple method for solving the inverse scattering problems in the resonance region, *Inverse Probl.* 12 (1996) 383–393.
- [12] D. Colton, M. Piana, R. Potthast, A simple method using Morozov's discrepancy principle for solving inverse scattering problems, *Inverse Probl.* 13 (1999) 1477–1493.
- [13] D. Colton, R. Kress, *Integral Equation Methods in Scattering Theory*, Wiley–Interscience, New York, 1983.
- [14] D. Colton, R. Kress, *Inverse Acoustic and Electromagnetic Scattering Theory*, Springer Verlag, New York, 1992.
- [15] M. Costabel, E. Stephan, A direct boundary integral equation method for transmission problems, *J. Math. Anal. Appl.* 106 (1985) 367–413.
- [16] H.W. Engl, M. Hanke, A. Neubauer, *Regularization of Inverse Problems*, Math. Appl., vol. 375, Kluwer Academic Publishers Group, Dordrecht, 1996.
- [17] M. Fares, S. Gratton, P. Toint, SVD-tail: a new linear-sampling reconstruction method for inverse scattering problems, *Inverse Probl.* 25 (2009) 1–19.
- [18] G.H. Golub, C.F. Van Loan, *Matrix Computations*, third ed., The Johns Hopkins University Press, Baltimore, MD, 1996.
- [19] C.W. Groetsch, *The Theory of Tikhonov Regularization for Fredholm Equations of the First Kind*, Pitman, Boston, 1984.
- [20] H. Haddar, P. Monk, The linear sampling method for solving the electromagnetic inverse medium problem, *Inverse Probl.* 18 (2002) 891–906.
- [21] P.C. Hansen, Regularization tools: a Matlab package for analysis and solution of discrete ill-posed problems, *Numer. Algorithms* 6 (1994) 1–35.
- [22] P.C. Hansen, *Rank-Deficient and Discrete Ill-Posed Problems*, SIAM, Philadelphia, 1998.
- [23] N.J. Higham, *Functions of Matrices: Theory and Computation*, SIAM, Philadelphia, 2008.

- [24] A. Kirsch, Characterization of the shape of a scattering obstacle using the spectral data of the far-field operator, *Inverse Probl.* 14 (1998) 1489–1512.
- [25] A. Kirsch, R. Kress, Uniqueness in inverse obstacle scattering, *Inverse Probl.* 9 (1993) 285–299.
- [26] R.E. Kleinman, P.A. Martin, On single integral equations for the transmission problem in acoustics, *SIAM J. Appl. Math.* 48 (1998) 307–325.
- [27] K.H. Leem, G. Pelekanos, F.S.V. Bazán, Fixed-point iterations in determining a Tikhonov regularization parameter in Kirsch’s factorization method, *Appl. Math. Comput.* 216 (2010) 3747–3753.
- [28] S. Lu, S.V. Pereverzev, Y. Shao, U. Tautenhahn, On the generalized discrepancy principle for Tikhonov regularization in Hilbert scales, *J. Integral Equations Appl.* 22 (2010) 483–517.
- [29] C.C. Paige, M.A. Saunders, LSQR: an algorithm for sparse linear equations and sparse least squares, *ACM Trans. Math. Software* 8 (1982) 43–71.
- [30] C.C. Paige, M.A. Saunders, LSQR: sparse linear equations and least squares problems, *ACM Trans. Math. Software* 8 (1982) 195–209.
- [31] G. Pelekanos, V. Sevroglou, Shape reconstruction of a 2D-elastic penetrable object via the L-curve method, *J. Inverse Ill-Posed Probl.* 14 (2006) 1–16.
- [32] U. Tautenhahn, Regularization of linear ill-posed problems with noisy right hand side and noisy operator, *J. Inverse Ill-Posed Probl.* 16 (2008) 507–523.
- [33] Y. Wang, A.G. Yagola, C. Yang (Eds.), *Optimization and Regularization for Computational Inverse Problems and Applications*, Springer-Verlag, Berlin, Heidelberg, 2010.